mice or rats empirically corresponds to half-lives that are 2 or 3 times longer in humans (Gabizon et al., 2003). In addition, the infusion dose of HbV as a RBC substitute, in terms of lipid content, is nearly a hundred times larger compared with other therapeutic uses of vesicles, even though HbV encapsulate a highly concentrated form of Hb (35–40 g/dl). Furthermore, there are many other factors such as the lipid formulation (Allen et al., 1989), vesicle size (Awasthi et al., 2003), and surface modification (Klibanov et al., 1990) that influence the circulation time and distribution of the infused vesicles. There are no clinical data available for using large infusion doses of vesicles such as those required for a RBC substitute. Therefore, we focused this research on determining the correlation factors between data from different species to simulate the pharmacokinetics of HbV. In addition, empty vesicles (EV) that do not contain Hb were studied as a reference to clarify the specific influence of encapsulated Hb on the circulation properties of the vesicles.

Scintigraphic imaging is a particularly powerful tool that can be used to develop and evaluate the formulation of vesicles (Goins and Phillips 2001). Using imaging, Phillips et al. have reported on the pharmacokinetics of liposome-encapsulated Hb radiolabeled with technetium-99m (^{99m}Tc) (Rudolph et al., 1991; Phillips et al., 1992, 1999) and achieved a formulation with long circulation times. These liposomes had a small size (<200 nm), neutral surface, and PEG modification (10 mol%), and were regarded as long-circulating vesicles (so-called stealth liposomes) ($t_{1/2}$ was 65 h after 25% intravenous top-load in rabbits) (Phillips et al., 1999). However, this particular liposome formulation had a low efficiency of Hb encapsulation, because the requisites for stealth liposomes, such as small size, neutral surface, and dense PEG modification were a disadvantage for efficient Hb encapsulation (Perkins et al., 1993; Nicholas et al., 2000). As mentioned above, the infused dose of RBC substitutes will be extremely high, so high encapsulation efficiency of Hb is essential for a successful oxygen-carrying RBC substitute. We have developed HbV with a lipid formulation and encapsulation conditions that have improved the encapsulation efficiency (Takeoka et al., 1996; Sou et al., 2003), and the present HbV formulation has an oxygen-carrying capacity equal to RBCs because of this higher encapsulation efficiency (1.7–2.0 g of Hb per gram of lipids). This article is the first report on the detailed pharmacokinetics of this HbV formulation using scintigraphic imaging of ^{99m}Tc-HbV for monitoring the circulation properties and biodistribution. Factors that would permit estimation of human pharmacokinetics of large quantities of vesicles are discussed.

Materials and Methods

Materials. 1,2-Dipalmitoyl-*sn*-glycero-3-phosphocholine (DPPC), cholesterol, and 1,5-dihexadecyl-L-glutamate-*N*-succinic acid (DPEA) were purchased from Nippon Fine Chemical Co., Ltd. (Osaka, Japan); 1,2-distearoyl-*sn*-glycero-3-phosphoethanolamine-*N*-[monomethoxy poly(ethylene glycol) (5000)] (PEG-DSPE) was purchased from NOF Co. (Tokyo, Japan). DPPC, cholesterol, DPEA, and PEG-DSPE were dissolved in alcohol at a molar ratio of 5, 5, 1, and 0.033, respectively, atomized, and evaporated using a spray dryer (Cracks) to prepare a lipid powder, at Nippon Fine Chemical Co., Ltd. The mixed lipid powder was hydrated with NaOH solution, submitted to three cycles of freeze-thawing, and the resultant dispersion was then lyophilized at Kanto Chemical Co. (Tokyo, Japan). The Hb solution was obtained from outdated donated blood (Japanese Red Cross) according to the purification method described previously (Sakai et al., 2002). The Hb solution (oxyhemoglobin) was converted to carbonylHb by purging the solution with 100% carbon monoxide until testing proved conversion (99% < HbCO). The final concentration of Hb was adjusted to 40 g/dl. Homocysteine, pyridoxal-5′ phosphate (PLP), and glutathione were purchased from Sigma-Aldrich (St. Louis, MO).

Preparation of HbV. HbV were prepared according to a method described previously (Takeoka et al., 1996; Tsuchida, 1998; Sakai et al., 2001; Sou et al., 2003). All HbV preparation work was performed under sterile conditions. The purified carbonylHb solution (40 g/dl) containing 5 mM homocysteine and pyridoxal-5′ phosphate [PLP/Hb ratio of 2.5 (mol/mol)] was mixed with the lyophilized powder containing the mixed lipids (DPPC, cholesterol, DPEA, and PEG-DSPE). After controlling the size of the HbV with an extrusion method (final pore size of the filter, 0.22 μm, Fuji microfilter; Fuji Photo Film Co., Tokyo, Japan), the unencapsulated Hb was removed by three ultracentrifugation steps (10^5g, 30 min each). CarbonylHb was converted to OxyHb by exposure to visible light in an atmosphere of O_2. HbV were suspended in a physiological salt solution and filtered through sterilized filters (pore size, 0.45-μm Dismic; Toyo Roshi, Tokyo, Japan) and deoxygenated by bubbling with N_2 before storage (Sakai et al., 2000a). The control EV encapsulating glutathione (30 mM) was prepared using the same extrusion method.

Characterization of HbV and EV. The characteristics of HbV and EV are summarized in Table 1. The concentrations of Hb and phospholipid were determined by a cyanomethemoglobin method (Hemoglobin Test Wako; Wako Pure Chemicals, Tokyo, Japan) and the cholineoxidase method (Phospholipid C Test Wako; Wako Pure Chemicals), respectively. The encapsulation efficiency of Hb was represented as a w/w ratio of [Hb]/[lipid]. Methemoglobin and carbonylHb content were determined by spectrophotometry (Van Assendelft, 1970). The diameters of the resulting HbV (247 ± 44 nm) and EV (259 ± 32 nm) were determined using a submicron particle analyzer (N4SD; Beckman Coulter, Fullerton, CA). Endotoxin contamination was determined to be below 0.2 EU/ml by the *Limulus* assay test (Sakai et al., 2004a).

^{99m}Tc-Labeling of HbV and EV. Radiolabeling of HbV was performed according to a method described previously (Phillips et al., 1992). A saline solution of sodium [^{99m}Tc]pertechnetate (5 ml, 75 mCi) (Nycomed Amersham, San Antonio, TX) was injected into a vial containing lyophilized hexamethylpropyleneamine oxime (HMPAO, 0.5 mg, $SnCl_2$, 7.6 μg) (Ceretec; Amersham Biosciences Inc., Piscataway, NJ). The mixed solution was incubated for 5 min at room temperature. The ^{99m}Tc-HMPAO solution (1 ml) was then added to the HbV suspension ([Hb]; 10 g/dl, 1 ml), and the resulting mixed solution was incubated for 1 h. After removing free ^{99m}Tc-HMPAO by gel filtration (Sephadex-G25 column), total radioactivity was measured in a dose calibrator (Mark 5 model; Radex, Houston, TX) and the labeling efficiency (E) was calculated as the percentage of post-radioactivity in ^{99m}Tc-HbV to preradioactivity. The ^{99m}Tc-HbV suspension was mixed with unlabeled HbV suspension and the resultant HbV suspension ([Hb], 9.5 g/dl; [lipid], 4.75 g/dl) was used for the experiment. The ^{99m}Tc-EV were also prepared with same method and the lipid concentration was adjusted to the same lipid concentration as that of HbV suspension tested ([lipid], 4.75 g/dl). The ^{99m}Tc-labeled HbV and EV dispersion (0.5 ml) was mixed with rat

TABLE 1
Characteristics of ^{99m}Tc-HbV and ^{99m}Tc-EV suspensions

Parameter	^{99m}Tc-HbV	^{99m}Tc-EV
[Hb][a] (g/dl)	9.5	0
[Lipids] (g/dl)	4.75	4.75
Particle diameter (nm)	247 ± 44	259 ± 32
Endotoxin level (EU/ml)	< 0.2	< 0.2

[a] Methemoglobin, <1%; carbonylHb, <2%.

plasma (1.5 ml) from a donor rat and incubated at 37°C to check the labeling stability. A 100-μl aliquot of incubated sample at 48 h after mixing was passed through a Bio Gel A-15m (200–400 mesh) spin column. The sample was eluted by sequential addition of 100 μl of Dulbecco's phosphate-buffered saline (pH 7.3) under the centrifugal force of 1000 rpm for 1 min. Each fraction was collected separately and counted in a scintillation well counter (Canberra multichannel analyzer; Canberra Industries, Meriden, CT). Another 100-μl aliquot of incubation sample was used as a standard. The sum total of activity eluted with HbV or EV fractions was compared with total radioactivity in the standard.

Animal Experiments. Animal experiments were performed under the National Institutes of Health Animal Use and Care guidelines and approved by the University of Texas Health Science Center at San Antonio Institutional Animal Care Committee. Male Sprague-Dawley rats (200–274 g) were anesthetized with 3% isoflurane (VedCo, St. Joseph, MO) in 100% oxygen gas. Rats were then placed in the supine position under a Picker (Cleveland, OH) large-field-of-view gamma camera using a low-energy, all-purpose collimator and interfaced with a Pinnacle imaging computer (Medasys, Ann Arbor, MI). Image acquisition was begun as HbV or EV were infused into the tail vein at 1 ml/min. Each rat received a total dose of 0.17 to 0.37 mCi of ^{99m}Tc activity, Hb: 1.33 g/kg b.wt.; lipids: 0.67 g/kg b.wt. as an equivalent of 14 ml/kg for the HbV group (n = 5) and 0.48 to 0.55 mCi of ^{99m}Tc activity, lipids: 0.67 g/kg as 14 ml/kg for the EV group (n = 5). The infused dose (in volume) was estimated to be 25% of blood volume where the total blood volume was assumed to be 5.6% of body weight (Frank, 1976). The rabbit experiment was performed in the same manner. Male New Zealand White rabbits (2.2–2.9 kg) were anesthetized with an intramuscular injection of ketamine/xylazine (both from Phoenix Scientific, St. Joseph, MO) mixture (50 and 10 mg/kg body weight, respectively). One ear of a rabbit was catheterized with a venous line, and the other ear was catheterized with an arterial line. HbV or EV was infused in the venous line at 1 ml/min under the same gamma camera, and the blood samples were drawn from the arterial line. Each rabbit received a total dose of 3.7 to 4.5 mCi of ^{99m}Tc activity, Hb: 1.36 g/kg b.wt.; lipids: 0.68 g/kg b.wt. as 14.25 ml/kg for the HbV group (n = 5) and 3.5 to 4.9 mCi, lipids: 0.68 g/kg as 14.25 ml/kg for the EV group (n = 4). The infused dose (in volume) was estimated to be 25% of blood volume where the total blood volume was assumed to be 5.7% of body weight (Kozma et al., 1974).

Image Analysis. One-minute dynamic 64 × 64 pixel scintigraphic images were acquired over a continuous period of 0.5 and 2 h for rats and rabbits after the infusion of HbV or EV, respectively. Static images were also acquired at 3, 6, 12, 24, 36, and 48 h postinfusion. The image analysis was performed using a nuclear medicine analysis workstation (Pinnacle computer; Medasys). The regions of interest were drawn over the whole body, liver, and spleen in images. The counts of radioactivity were decay-corrected at each time and converted to a percentage of the whole body counts. Corrections were made for the blood pool contribution of the liver and spleen of the rat (17 and 6%, respectively, of the total blood volume). For rabbit, the liver was corrected by 25.4% of the total blood volume, and the spleen was individually corrected by 1.047 ± 0.076% for HbV and 1.592 ± 0.049% of the total blood volume for EV as percentage of infused dose (%ID) just after infusion, respectively.

Blood Persistence and Biodistribution. Blood was collected from the tail vein of the rat or arterial line of the rabbit (50 or 100 μl) at various times postinfusion. The radioactivity of blood samples was quantified in a scintillation well counter (Canberra multichannel analyzer; Canberra Industries) at the same time. The counts at each time were converted to the percentage of the counts of sample collected immediately after infusion. The elimination rate constants (k) were calculated by the least-squares method and half-life time ($t_{1/2}$) was calculated from eq. 1.

$$t_{1/2} = \frac{0.693}{k} \quad (1)$$

The animals were rapidly sacrificed at 48 h, and the tissue samples were collected, weighed, and counted for radioactivity in a scintillation well counter (Canberra multichannel analyzer; Canberra Industries) to calculate the biodistribution. To calculate the %ID per organ, total blood volume, muscle, and skin mass were estimated as 5.6, 40, and 13% of total body weight for rat (Frank, 1976; Petty, 1982), and 5.7, 45, and 10% of total body weight for rabbit (Kozma et al., 1974; Kaplan and Timmons, 1979), respectively. The bone was estimated as 10% of total body weight for rat (Frank, 1976; Petty, 1982) and 12 times the femur weight for rabbit (Dietz, 1944).

Estimation of the Biodistribution in Humans. The total Hb or lipids per organ (Ws) was calculated from the %ID and ID of Hb or lipids in terms of weight.

$$Ws(\text{mg}) = \frac{\%\text{ID} \times \text{ID}}{100} \quad (2)$$

The organ weight (Wo) of experimental animals was measured by an electronic balance and the Hb per organ weight (R) was calculated.

$$R(\text{mg/g}) = \frac{Ws}{Wo} \quad (3)$$

Ws was calculated from eq. 3 for humans, where the weights of liver, spleen, and bone (Wo) were estimated as 1.8, 0.18, and 5.0 kg, respectively, for average humans (70 kg) (International Commission on Radiological Protection, 1984), and the R value was applied as an average value between rats and rabbits shown in Table 4 for each organ. The ID of HbV ([Hb] = 9.5 g/dl, [lipids] = 4.75 g/dl) was calculated to be 25% of the blood volume (4.9 liters, 70 ml/kg b.wt.), and the %ID was calculated from eq. 2. The half-life times ($t_{1/2\beta}$) were estimated from eq. 4, where, constant value (C) was determined as a slope of the fitting line in this study and $\%\text{ID}_{\text{total}}$ was sum values of %ID for liver, spleen, and bone.

$$t_{1/2\beta} = \frac{C}{\%\text{ID}_{\text{total}}} \quad (4)$$

Statistical Methods. Values are reported as mean ± S.E.M. Statistical analysis was performed using Microsoft Excel for Windows. The image analysis and biodistribution data were compared using the Student's unpaired t test. A P value <0.01 or 0.05 was considered statistically significant.

Results

Labeling Efficiencies. The labeling efficiencies of ^{99m}Tc-HbV and ^{99m}Tc-EV were 69.1 ± 2.0% (n = 2) and 75.6 ± 5.1% (n = 3) for the rat studies, and 62.0 ± 4.8% (n = 5) and 70.9 ± 2.1% (n = 2) for the rabbit studies. Labeling efficiencies were similar for both ^{99m}Tc-HbV and ^{99m}Tc-EV, even though ^{99m}Tc-HbV used homocysteine and ^{99m}Tc-EV used glutathione. The ^{99m}Tc would be located in the inner aqueous phase of vesicles, and both homocysteine and Hb of HbV, and glutathione of EV would possibly bind the ^{99m}Tc (Rudolph et al., 1991; Phillips et al., 1992). The incubation of labeled HbV and EV in serum for 48 h revealed that 5 and 4% of the ^{99m}Tc dissociated from HbV and EV, indicating that the labeling was very stable and the contents were stably encapsulated inside the vesicles.

Circulation Kinetics. To determine the circulation kinetics as shown in Fig. 1, a and b, the radioactive counts of blood samples were plotted as a percentage of the counts for blood sample collected immediately at the end of the infusion with

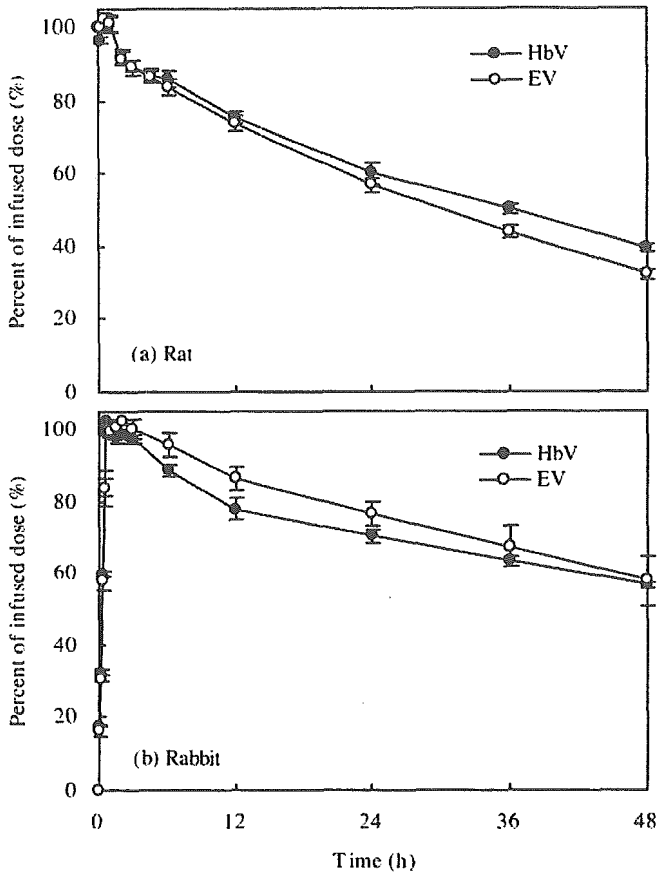

Fig. 1. Circulation kinetics of HbV and EV after top-loading intravenous infusion (14 ml/kg) in rats and rabbits. The radioactivity was determined by scintillation counting of blood samples with time. The percentage of radioactivity is calculated as a percentage of baseline radioactivity in a blood sample withdrawn just after HbV or EV infusion.

time. The elimination profiles of infused HbV showed two components with an initial fast clearance followed by a slower clearance phase, which is regarded as a distribution (α) phase in the mononuclear phagocyte system (MPS) and an elimination (β) phase, respectively. The clearance rate constant in the distribution phase of HbV was equal to that of EV, and k_β was 1.3 times smaller than that of EV in rats as shown in Table 2. The circulation half-life times ($t_{1/2}$ values) associated with both the distribution and elimination phases of HbV and EV in rats were 34.8 and 29.3 h, respectively. The clearance rates of HbV and EV were slower in rabbits compared with those in rats, especially for the distribution phase. The k_α of HbV was 0.0226 h^{-1} in rabbit, which was one-quarter of that in rats and 1.4 times larger than that of EV in rabbit. k_β for HbV was 1.3 times smaller than that of EV. The $t_{1/2}$ values of HbV and EV were 62.6 and 57.3 h in rabbits, respectively.

Imaging Study. The gamma camera images of rats or rabbits receiving HbV were acquired at various times to determine the organ distribution profiles with time. As shown in Figs. 2 and 3, radioactivity was observed over the whole body of animals and in the heart, demonstrating that HbV were circulating. Immediately after infusion, the heart, liver, and spleen were identified because these organs had a large blood pool volume, and the relative intensities of the liver and spleen increased in comparison with the heart with time. The %ID in liver and spleen calculated from gamma camera images with decay correction and correction for blood pool contribution are shown in Fig. 4. The %ID in liver was increased during the infusion and decreased after the infusion ended, especially in HbV as shown in Fig. 4, a and c. This initial decrease was most likely due to the adjustment of blood volume after top-loading. The values of %ID in liver and spleen were quickly increased during the first 6 to 12 h after infusion and reached a plateau at 48 h. At 48 h, the liver had 10.9 ± 0.8 and 7.6 ± 1.0% of HbV in rats and rabbits, respectively, whereas the spleen had 6.6 ± 0.3 and 0.98 ± 0.14% of HbV in rats and rabbits, respectively.

Biodistribution. The detailed biodistribution data of HbV at 48 h are shown in Table 3. HbV could be precipitated easily by ultracentrifugation of blood sample, and no Hb was detected in the supernatant serum in the blood sample for 48 h. In addition, no Hb was detected in urine for 48 h supporting that the Hb was not eluted from vesicles during circulation. HbV and EV were mainly distributed in liver, bone marrow, and spleen, and the %ID values for HbV were smaller than those of EV in these organs. Relatively high values for the bowel, feces, and urine were likely due to metabolism during excretion of HbV. The sum values of %ID for liver, spleen, and bone ($\%ID_{total}$), which are the main organs for MPS uptake, were 26.60 and 13.64% for HbV and 36.36 and 17.84% for EV in rats and rabbit, respectively. The corresponding $t_{1/2\beta}$ values given in Table 2 were 39.1, 79.2, 30.1, and 60.2 h, respectively. These $t_{1/2\beta}$ values are in proportion to the reciprocal of $\%ID_{total}$ as shown in Fig. 5, and the constant value (C) in eq. 4 was determined to be 1074.1 as a slope of the fitting line.

The calculated total lipids and Hb doses (in milligrams) delivered to the liver, bone, and spleen are summarized in Table 4. These values are independent of the species dependence of relative weight balances of organs in whole body and represent the amount of uptake of the HbV in a gram of each organ. The spleen had 14.43 ± 0.54 and 14.92 ± 1.25 mg of Hb per gram in rat and rabbit, and the liver and bone also had similar values in rat and rabbit.

Discussion

The improvement in oxygen-carrying capacity of HbV as a RBC substitute requires longer circulation and a higher en-

TABLE 2
Kinetic parameters of HbV and EV clearance from blood in rats and rabbits (25% top-loading)

Animal	Sample	Distribution (α) Phase		Elimination (β) Phase		$t_{1/2}$
		k_α	$t_{1/2\alpha}$	k_β	$t_{1/2\beta}$	
		h^{-1}	h	h^{-1}		h
Rat	HbV	0.0894	7.8	0.0177	39.1	34.8
	EV	0.1004	6.9	0.0230	30.1	29.3
Rabbit	HbV	0.0226	30.7	0.0088	79.2	62.6
	EV	0.0159	43.6	0.0115	60.2	57.3

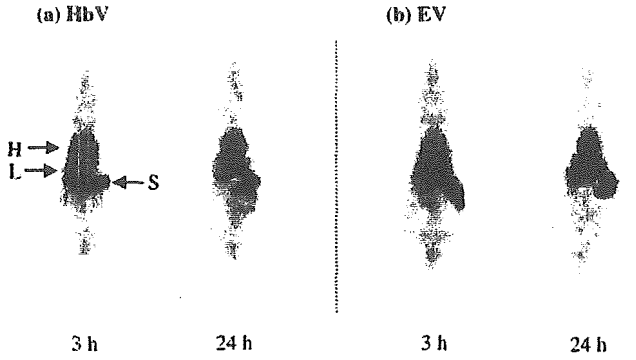

Fig. 2. Static gamma camera images of whole body of rats infused with HbV or EV acquired at 3 and 24 h after infusion. The images were acquired for 1 min at 3 h and 2 min at 24 h. The arrows show heart (H), liver (L), and spleen (S).

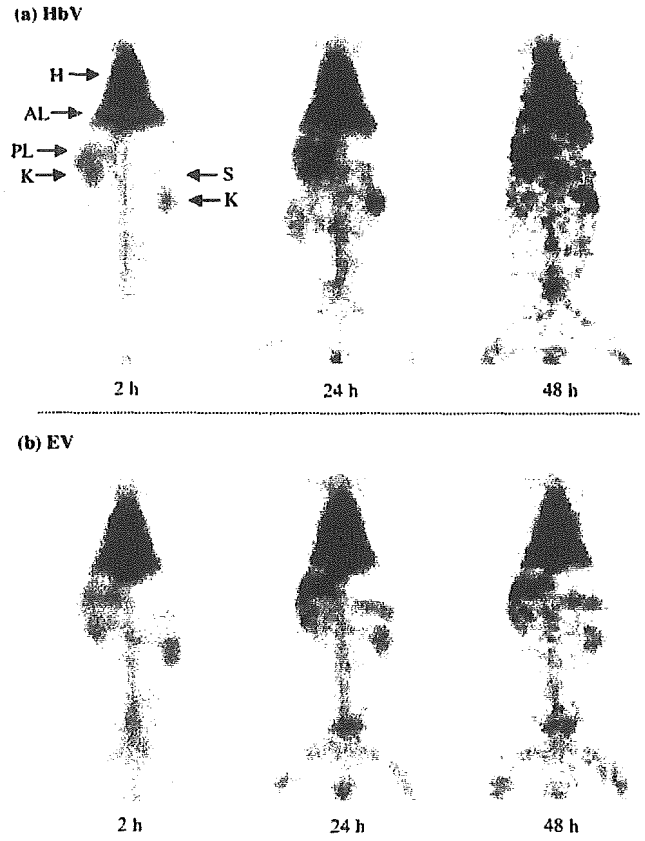

Fig. 3. Static gamma camera images of rabbits acquired at 2, 24, and 48 h after HbV or EV infusion. The images were acquired for 1 min at 2 h, 2 min at 24 h, and 5 min at 48 h. The arrows indicate heart (H), anterior liver (AL), posterior liver (PL), spleen (S), and kidney (K).

capsulation efficiency of Hb. The HbV formulation described in this study has high encapsulation efficiency ([Hb]/[lipid] = 2.0), and a circulatory half-life time of 34.8 and 62.6 h in rats and rabbits, respectively. This value is equal to the 65-h circulation half-life time for a PEG-liposome-encapsulated Hb formulation with a long circulation time in rabbits (Phillips et al., 1999). Other long-circulation vesicle formulations are successful for therapeutic uses such as cancer therapy or antibacterial treatment (Papahadjopoulos et al., 1991; Gabizon et al., 2003). However, the characteristics of small size (below 200 nm), neutral surface, and incorporation of significant amounts of PEG-lipid (5–10 mol%) of these formulations are ineffective in encapsulating Hb into vesicles (Perkins et al., 1993; Nicholas et al., 2000). The HbV formulation described in the present study is mainly composed of DPPC and cholesterol, only 0.3 mol% of PEG-lipid to prevent aggregation of the vesicles (Sakai et al., 2000a; Sou et al., 2000), and 9 mol% of anionic DPEA to reduce the lamellarity of the bilayer membrane (Sou et al., 2003). In general, anionic phospholipids such as phosphatidylglycerol or phosphatidylserine are used for the preparation of anionic vesicles; however, some side effects such as complement and platelet activations have been reported (Reinish et al., 1988). These immunological responses accelerate plasma protein adsorption on the surface of vesicles (opsonins) and then those vesicles are rapidly trapped into MPS. Our DPEA has a carboxylic group to negatively charge the surface of vesicles instead of a phosphate group of anionic phospholipids, and it does not have side effects like those reported for phosphatidylglycerol-containing vesicles (Wakamoto et al., 2001). The safety studies of HbV are underway, and the initial results in rats suggest that the DPEA vesicles have fewer side effects on immunological responses such as complement activation and thrombocytopenia compared with vesicles containing other anionic phospholipids. This bioinactive surface imparted by DPEA contributes to the stable circulation of HbV.

The diameter of vesicles is also an important factor for circulation kinetics and encapsulation efficiency. Recently, Awasthi et al. (2003) reported that the maximum size to show long circulation characteristics of PEG vesicle was around 240 nm in rabbits. The larger size of HbV is advantageous for the encapsulation efficiency of Hb; however, 250-nm HbV is of maximum and reasonable size to satisfy both long circulation and high Hb content requirements. We satisfied both long-circulation and high encapsulation efficiency of Hb by developing the lipid formulation and strictly regulating the diameter by the extrusion method. The clear effect of encapsulated Hb on the circulation time of vesicles was prolongation of the β phase for both animals. This is most likely due to greater saturation of the MPS by the encapsulated Hb.

Biodistribution data showed that HbV and EV were mainly distributed into liver, spleen, and bone. We have already clarified that Hb and phospholipid from HbV readily disappeared from the Kupffer cells in liver and macrophages in spleen in rats within a week after administration (Sakai et al., 2001). The trapping of HbV in MPS is regarded as a normal physiological pathway for removal of aged RBC; therefore, this should be a reasonable pathway for the elimination and metabolism of Hb-based RBC substitutes. The importance of the biodistribution of Hb-based RBC substitutes has been discussed and a vasoconstrictive effect of modified Hbs has been indicated (Sakai et al., 2000b). These side effects are triggered by the unusual biodistribution of small-sized modified Hb (<100 nm) to smooth muscle across the endothelium or the space of Disse in fenestrated endothelium of hepatic sinusoids, where the vasorelaxation factors nitric oxide and carbon monoxide are bound to Hb (Goda et al., 1998). The smaller vesicles might be effective for longer circulation of encapsulated Hb, but this would have the risk of causing similar or unusual side effects as those observed for modified Hb.

As summarized in Table 3, the %ID of HbV and EV in biodistribution data at 48 h is significantly different between

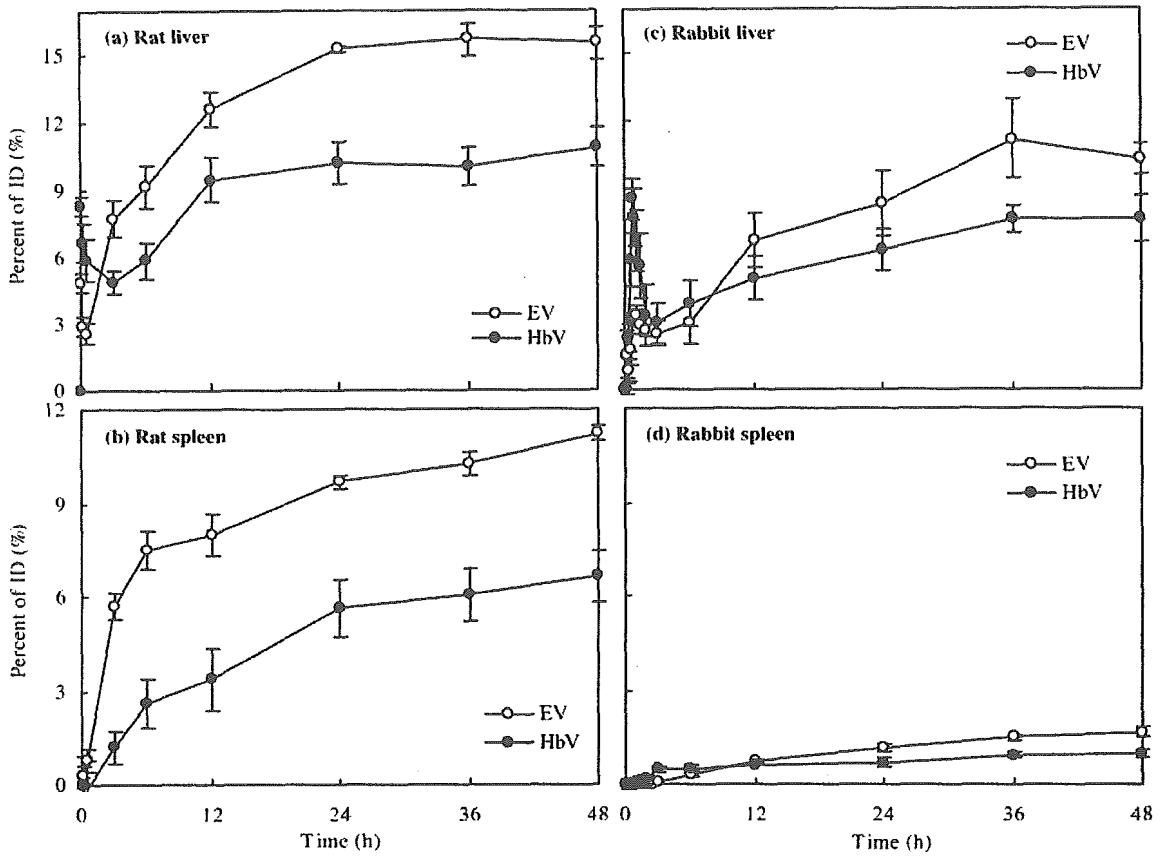

Fig. 4. %ID for liver and spleen calculated from the gamma camera image acquired at particular times and after decay correction. The blood pool contribution was corrected using values of 17 and 6% of the total blood volume for liver and spleen in rats, respectively. For rabbit, the liver was corrected by 25.4% of the total blood volume, and the spleen was individually corrected by 1.047 ± 0.076% for HbV and 1.592 ± 0.049% of the total blood volume for EV as %ID of just after infusion, respectively.

rats and rabbits ($P < 0.05$ for many organs). The rat had more HbV and EV in liver, bone, and especially spleen and less HbV and EV in blood. These data suggest that the biodistribution pattern of vesicles was not specifically changed by the encapsulation of Hb or the animal species tested; however, the quantitative values of %ID were significantly affected by these factors. Image analysis showed that the %ID required for saturating the liver and spleen with time was as shown in Fig. 4. The former liposome encapsulated Hb, which had non-PEG, showed significantly greater %ID (liver, 15.4 ± 2.1% ID; spleen, 18.1 ± 3.3% ID) in rabbit (Rudolph et al., 1991). The "saturated" level observed at those infusion doses would be determined by the balance between rate of uptake from the circulation, which was strongly affected by the HbV formulation and the rate of metabolic processing. The full saturation of MPS by the increased infusion dose of HbV might diminish the difference of pharmacokinetics between HbV formulations because the metabolic processing should become dominant factor. At 48 h, the blood clearance was in the slower β phase (Fig. 1) so that the inverse proportion between %ID and $t_{1/2\beta}$ is reasonable, and the determined constant C is available to estimate the $t_{1/2\beta}$ from the %ID. In addition, we have discovered that the most important factor for explaining the difference of %ID accumulating in the organs of the MPS between species is due to the different ratio of organ weight to body weight between species. For example, the average spleen weights of the experimental animals for HbV were 0.65 ± 0.07g in rats (216 ± 20 g b.wt., $n = 5$) and 0.87 ± 0.21 g in rabbits (2670 ± 97 g b.wt., $n = 5$). Therefore, the ratio of organ weight to body weight of rats is 9 times larger than that of rabbits, which means that rats have a 9 times larger mass capacity in spleen at the same infusion dose based on body weight. When the uptake of HbV is calculated in terms of mg of lipid and Hb per gram of MPS organ, the values in rats and rabbits are very close to each other as summarized in Table 4, indicating that the concentration of HbV in these organs was species-independent in this case. These values can be used to quantitatively estimate biodistribution of HbV based on organ weight. By using these two factors of C values and milligrams of lipids per organ weight, we were able to roughly estimate the biodistribution and circulation time of HbV in humans (see *Materials and Methods*). Laverman et al. (2000) reported that the distribution pattern of PEG-liposomes in humans was similar to that of rats and rabbits, with high uptake in liver, spleen, and bone marrow. Other biodistribution studies of vesicles also suggested a high uptake in liver, spleen, and bone marrow in humans (Dams et al., 2000; Gabizon et al., 2003), and these reports support our estimation. Based on the MPS organ weights of average humans and the milligrams of uptake of lipid and hemoglobin per gram MPS organs at 48 h (human liver weight, 1.8 kg; human spleen, 0.18 kg; and human bone, 5.0 kg) (International Commission on Radiological Protection, 1984), we estimated that %IDs of HbV are 5.4% (liver), 4.5% (spleen), and 6.4% (bone), and a $t_{1/2\beta}$ of approximately 66 h in humans after a 25% top-loading

TABLE 3
Biodistribution of HbV and EV as a percentage of the infused dose per organ (%ID/organ) and percentage of the infused dose per gram of organ (%ID/g organ) at 48 h after 25% top-loading in rats or rabbits

Organ	Rat		Rabbit	
	HbV	EV	HbV	EV
%ID/organ ± S.E.M.				
Blood	33.27 ± 1.11*	24.13 ± 0.65	50.95 ± 2.02†	52.76 ± 4.80‡
Liver	10.04 ± 0.86*	14.13 ± 0.40	7.55 ± 0.46†	8.64 ± 0.34‡
Bone	10.06 ± 0.21*	13.05 ± 0.38	5.37 ± 0.33*†	7.36 ± 0.28‡
Spleen	6.50 ± 0.30*	9.18 ± 0.37	0.72 ± 0.10*†	1.84 ± 0.28‡
Bowels	7.30 ± 1.59	4.16 ± 0.35	9.61 ± 2.31	8.62 ± 4.42
Skin	2.37 ± 0.33	2.29 ± 0.12	0.88 ± 0.05†	1.09 ± 0.21‡
Kidney	2.40 ± 0.10*	3.35 ± 0.08	1.47 ± 0.13†	1.69 ± 0.21‡
Muscle	1.94 ± 0.28	1.98 ± 0.27	2.51 ± 0.31	2.62 ± 0.76
Lung	0.62 ± 0.03	0.54 ± 0.03	0.55 ± 0.02	0.43 ± 0.06
Heart	0.17 ± 0.01	0.16 ± 0.01	0.12 ± 0.01†	0.13 ± 0.02
Brain	0.16 ± 0.01*	0.09 ± 0.01	0.08 ± 0.01*†	0.05 ± 0.00‡
Testis	0.12 ± 0.01*	0.09 ± 0.01	0.06 ± 0.02†	0.07 ± 0.01
Feces	9.50 ± 1.17	6.95 ± 0.29	5.06 ± 2.56	2.02 ± 0.55‡
Urine	13.61 ± 0.31	12.87 ± 0.41	11.30 ± 1.22	7.81 ± 1.44‡
%ID/g organ ± S.E.M.				
Blood	2.919 ± 0.032	1.706 ± 0.044	0.356 ± 0.017	0.354 ± 0.030
Liver	1.244 ± 0.096	1.378 ± 0.045	0.093 ± 0.004	0.131 ± 0.019
Bone	0.497 ± 0.021	0.518 ± 0.020	0.043 ± 0.003	0.062 ± 0.002
Spleen	10.059 ± 0.072	10.790 ± 0.402	0.823 ± 0.072	1.483 ± 0.072
Bowels	0.390 ± 0.073	0.202 ± 0.008	0.031 ± 0.006	0.029 ± 0.014
Skin	0.091 ± 0.014	0.070 ± 0.004	0.004 ± 0.000	0.004 ± 0.001
Kidney	1.604 ± 0.057	1.839 ± 0.055	0.089 ± 0.005	0.110 ± 0.017
Muscle	0.024 ± 0.003	0.020 ± 0.003	0.002 ± 0.000	0.002 ± 0.001
Lung	0.619 ± 0.022	0.458 ± 0.014	0.068 ± 0.004	0.057 ± 0.012
Heart	0.264 ± 0.009	0.187 ± 0.012	0.026 ± 0.002	0.027 ± 0.006
Brain	0.111 ± 0.010	0.062 ± 0.003	0.011 ± 0.001	0.006 ± 0.001
Testis	0.042 ± 0.002	0.027 ± 0.001	0.013 ± 0.002	0.016 ± 0.003

* Difference is statistically significant from EV in same species at $P < 0.01$.
† Difference is statistically significant from HbV in rat at $P < 0.05$.
‡ Difference is statistically significant from EV in rat at $P < 0.05$.

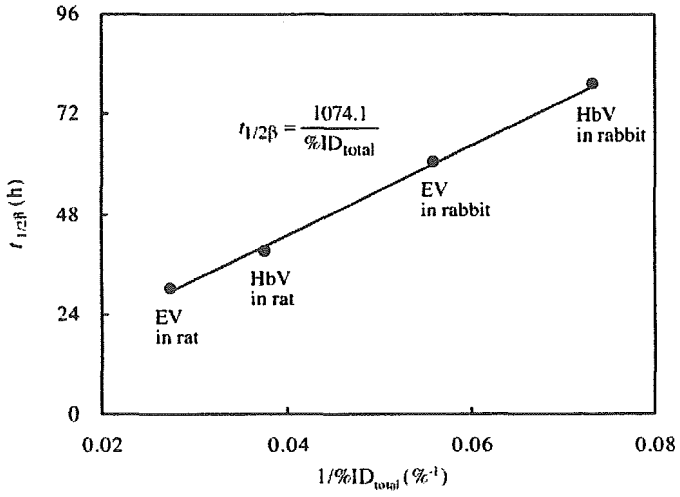

Fig. 5. Proportional relationship between the circulation half-life time ($t_{1/2\beta}$) and the reciprocal of $\%ID_{total}$ in the elimination phase. The $\%ID_{total}$ was calculated as a sum value of %ID in liver, bone, and spleen at 48 h. The fitting line was determined by the regression analysis (coefficient of determination; $R^2 = 0.9985$).

([Hb], 9.5 g/dl; [lipid], 4.75 g/dl). The normal range of human organ weight is relatively wide such as 1.4 to 1.8 kg (liver) and 0.08 to 0.3 kg (spleen), so the $t_{1/2\beta}$ would be varied around 3 days. This $t_{1/2\beta}$ is approximately two times larger than that of rat, and this ratio almost follows that derived from empirical speculation (Gabizon et al., 2003). This method of estimating vesicle circulation kinetics and organ uptake in different animal species may be useful for all types of vesicle (liposome) formulations that are currently under development as drug delivery vehicles. More studies will be required to further validate this method of estimating circulation kinetics and organ uptake in different animal species.

The development of RBC substitutes is progressing, and some modified Hbs have been studied in clinical trials. The reported $t_{1/2}$ value was 23 h for polymerized bovine Hb (Hughes et al., 1995), 16 to 20 h for *o*-raffinose-cross-linked and polymerized human Hb (Carmichael et al., 2000), and 24 h for glutaraldehyde-cross-linked and polymerized human Hb (Gould et al., 1998). Even though HbV have not yet been tested clinically, we have demonstrated in the present report that HbV have significantly improved properties, based on their circulation kinetics and biodistribution, suggesting their improved safety and efficacy as a RBC substitute. In addition, the successful application of vesicles as RBC substitutes at this large infusion dose suggests a promising future for vesicles (liposomes), and the present formulation would potentially be available not only as a RBC substitute but also for various applications such as drug delivery systems.

Acknowledgments

We gratefully acknowledge Drs. S. Takeoka and H. Sakai (Waseda University) for discussion of the experimental points and cooperation to promote this collaborative research between Waseda University and University of Texas Health Science Center at San Antonio, Y. Naito and M. Masada (Waseda University) for supporting the HbV preparation, and Dr. V. D. Awasthi (University of Texas Health Science Center at San Antonio) for advice on the experimental techniques.

TABLE 4
Comparison of HbV and EV as milligrams of lipids per gram of organ and milligrams of Hb per gram of organ at 48 h after 25% top-loading in rats or rabbits

Organ	HbV in Rat		HbV in Rabbit		EV in Rat	EV in Rabbit
	mg lipids/g organ[a]	*mg Hb/g organ*[b]	*mg lipids/g organ*[a]	*mg Hb/g organ*[b]	*mg lipids/g organ*[a]	
Blood	4.23 ± 0.20	8.40 ± 0.40	6.47 ± 0.24[†]	12.93 ± 0.48[†]	2.94 ± 0.06	6.55 ± 0.64[†]
Liver	1.79 ± 0.12	3.56 ± 0.23	1.68 ± 0.06	3.36 ± 0.12	2.38 ± 0.06	2.24 ± 0.18
Bone	0.72 ± 0.01	1.42 ± 0.02	0.78 ± 0.05	1.57 ± 0.09	0.89 ± 0.04	1.09 ± 0.08
Spleen	14.43 ± 0.54	28.63 ± 1.06	14.92 ± 1.25	29.85 ± 2.50	18.58 ± 0.51	25.83 ± 1.43[†]

[†] Difference is statistically significant from HbV in rat at $P < 0.05$.
[a] Calculated values from ID of lipids and %ID/g organ.
[b] Calculated values from ID of Hb and %ID/g organ.

References

Allen TM, Hansen C, and Rutledge J (1989) Liposomes with prolonged circulation times: factors affecting uptake by reticuloendothelial and other tissues. *Biochim Biophys Acta* **981**:27–35.

Awasthi VD, Garcia D, Goins BA, and Phillips WT (2003) Circulation and biodistribution profiles of long-circulating PEG-liposomes of various sizes in rabbits. *Int J Pharm* **253**:121–132.

Carmichael FJ, Ali AC, Campbell JA, Langlois SF, Biro GP, Willan AR, Pierce CH, and Greenburg AG (2000) A phase I study of oxidized raffinose cross-linked human hemoglobin. *Crit Care Med* **28**:2283–2292.

Dams ET, Oyen WJ, Boerman OC, Storm G, Laverman P, Kok PJ, Buijs WC, Bakker H, van der Meer JW, and Corstens FH (2000) 99mTc-PEG liposomes for the scintigraphic detection of infection and inflammation: clinical evaluation. *J Nucl Med* **41**:622–630.

Dietz AA (1944) Distribution of bone marrow, bone and bone ash in rabbits. *Proc Soc Exp Biol Med* **57**:60–62.

Djordjevich L and Miller IF (1980) Synthetic erythrocytes from lipid encapsulated hemoglobin. *Exp Hematol* **8**:584–592.

Frank DW (1976) Physiological data of laboratory animals, in *Handbook of Laboratory Animals Science* (Melby ECJ ed) pp 23–64, CRC Press, Boca Raton, FL.

Gaber BP and Farmer MC (1984) Encapsulation of hemoglobin in phospholipid vesicles: preparation and properties of a red cell surrogate. *Prog Clin Biol Res* **165**:179–190.

Gabizon A, Shmeeda H, and Barenholz Y (2003) Pharmacokinetics of pegylated liposomal doxorubicin: review of animal and human studies. *Clin Pharmacokinet* **42**:419–436.

Goda N, Suzuki K, Naito M, Takeoka S, Tsuchida E, Ishimura Y, Tamatani T, and Suematsu M (1998) Distribution of heme oxygenase isoforms in rat liver. Topographic basis for carbon monoxide-mediated microvascular relaxation. *J Clin Investig* **101**:604–612.

Goins BA and Phillips WT (2001) The use of scintigraphic imaging as a tool in the development of liposome formulations. *Prog Lipid Res* **40**:95–123.

Gould SA, Moore EE, Hoyt DB, Burch JM, Haenel JB, Garcia J, DeWoskin R, and Moss GS (1998) The first randomized trial of human polymerized hemoglobin as a blood substitute in acute trauma and emergent surgery. *J Am Coll Surg* **187**:113–122.

Gregoriadis G and Neerunjun D (1974) Control of the rate of hepatic uptake and catabolism of liposome-entrapped proteins injected into rats. Possible therapeutic applications. *Eur J Biochem* **47**:179–185.

Hughes GS Jr, Yancey EP, Albrecht R, Locker PK, Francom SF, Orringer EP, Antal EJ, and Jacobs EE Jr (1995) Hemoglobin-based oxygen carrier preserves submaximal exercise capacity in humans. *Clin Pharmacol Ther* **58**:434–443.

International Commission on Radiological Protection (1984) Report on the task group on reference man. ICRP No. 23. Pergamon Press, New York.

Kaplan HM and Timmons EH (1979) *The Rabbit: A Model for the Principles of Mammalian Physiology and Surgery*, Academic Press, New York.

Klibanov AL, Maruyama K, Torchilin VP, and Huang L (1990) Amphipathic polyethyleneglycols effectively prolong the circulation time of liposomes. *FEBS Lett* **268**:235–237.

Kozma C, Macklin W, Cummins LM, and Mauer R (1974) Anatomy, physiology, and biochemistry of the rabbit, in *The Biology of the Laboratory Rabbit* (Weisbroth SH, Flatt RE, and Kraus AL eds) pp 50–69, Academic Press, New York.

Laverman P, Brouwers AH, Dams ET, Oyen WJ, Storm G, van Rooijen N, Corstens FH, and Boerman OC (2000) Preclinical and clinical evidence for disappearance of long-circulating characteristics of polyethylene glycol liposomes at low lipid dose. *J Pharmacol Exp Ther* **293**:996–1001.

Nicholas AR, Scott MJ, Kennedy NI, and Jones MN (2000) Effect of grafted polyethylene glycol (PEG) on the size, encapsulation efficiency and permeability of vesicles. *Biochim Biophys Acta* **1463**:167–178.

Papahadjopoulos D, Allen TM, Gabizon A, Mayhew E, Matthay K, Huang SK, Lee KD, Woodle MC, Lasic DD, Redemann C, et al. (1991) Sterically stabilized liposomes: improvements in pharmacokinetics and antitumor therapeutic efficacy. *Proc Natl Acad Sci USA* **88**:11460–11464.

Perkins WR, Minchey SR, Ahl PL, and Janoff AS (1993) The determination of liposome captured volume. *Chem Phys Lipids* **64**:197–217.

Petty C (1982) *Research Techniques in the Rat*, pp 66–70, Charles C. Thomas, Springfield, IL.

Phillips WT, Klipper RW, Awasthi VD, Rudolph AS, Cliff R, Kwasiborski V, and Goins BA (1999) Polyethylene glycol-modified liposome-encapsulated hemoglobin: a long circulating red cell substitute. *J Pharmacol Exp Ther* **288**:665–670.

Phillips WT, Rudolph AS, Goins B, Timmous JH, Klipper R, and Blumhardt R (1992) A simple method for producing a technetium-99m-labeled liposome which is stable in vivo. *Nucl Med Biol* **19**:539–547.

Reinish LW, Bally MB, Loughrey HC, and Cullis PR (1988) Interactions of liposomes and platelets. *Thromb Haemost* **60**:518–523.

Rudolph AS, Klipper RW, Goins B, and Phillips WT (1991) In vivo biodistribution of a radiolabeled blood substitute: 99mTc-labeled liposome-encapsulated hemoglobin in an anesthetized rabbit. *Proc Natl Acad Sci USA* **88**:10976–10980.

Sakai H, Hisamoto S, Fukutomi I, Sou K, Takeoka S, and Tsuchida E (2004a) Detection of lipopolysaccharide in hemoglobin-vesicles by *Limulus* amebocyte lysate test with kinetic-turbidimetric gel clotting analysis and pretreatment of surfactant. *J Pharm Sci* **93**:310–321.

Sakai H, Horinouchi H, Tomiyama K, Ikeda E, Takeoka S, Kobayashi K, and Tsuchida E (2001) Hemoglobin-vesicles as oxygen carriers: influence on phagocytic activity and histopathological changes in reticuloendothelial system. *Am J Pathol* **159**:1079–1088.

Sakai H, Masada Y, Horinouchi H, Yamamoto M, Ikeda E, Takeoka S, Kobayashi K, and Tsuchida E (2004b) Hemoglobin-vesicles suspended in recombinant human serum albumin for resuscitation from hemorrhagic shock in anesthetized rats. *Crit Care Med* **32**:539–545.

Sakai H, Masada Y, Takeoka S, and Tsuchida E (2002) Characteristics opf bovine hemoglobin as a potential source of hemoglobin-vesicles for an artificial oxygen carrier. *J Biochem* **131**:611–617.

Sakai H, Tomiyama KI, Sou K, Takeoka S, and Tsuchida E (2000a) Poly(ethylene glycol)-conjugation and deoxygenation enable long-term preservation of hemoglobin-vesicles as oxygen carriers in a liquid state. *Bioconjug Chem* **11**:425–432.

Sakai H, Yuasa M, Onuma H, Takeoka S, and Tsuchida E (2000b) Synthesis and physicochemical characterization of a series of hemoglobin-based oxygen carriers: objective comparison between cellular and acellular types. *Bioconjug Chem* **11**:56–64.

Savitsky JP, Doczi J, Black J, and Arnold JD (1978) A clinical safety trial of stroma-free hemoglobin. *Clin Pharm Ther* **23**:73–80.

Sou K, Endo T, Takeoka S, and Tsuchida E (2000) Poly(ethylene glycol)-modification of the phospholipid vesicles by using the spontaneous incorporation of poly(ethylene glycol)-lipid into the vesicles. *Bioconjug Chem* **11**:372–379.

Sou K, Naito Y, Endo T, Takeoka S, and Tsuchida E (2003) Effective encapsulation of proteins into size-controlled phospholipid vesicles using the freeze-thawing and extrusion. *Biotechnol Prog* **19**:1547–1552.

Takeoka S, Ohgushi T, Terase K, Ohmori T, and Tsuchida E (1996) Layer-controlled hemoglobin vesicles by interaction of hemoglobin with a phospholipid assembly. *Langmuir* **12**:1755–1759.

Takeoka S, Teramura Y, Atoji T, and Tsuchida E (2002) Effect of Hb-encapsulation with vesicles on H_2O_2 reaction and lipid peroxidation. *Bioconjug Chem* **13**:1302–1308.

Tsuchida E (ed) (1998) *Blood Substitute: Present and Future Perspective*, Elsevier Science, Amsterdam.

Van Assendelft OW (1970) *Spectrophotometry of Haemoglobin Derivatives*, pp 125–129, Royal Vangorcum Ltd., Assen, The Netherlands.

Wakamoto S, Fujihara M, Abe H, Sakai H, Takeoka S, Tsuchida E, Ikeda H, and Ikebuchi K (2001) Effects of poly(ethyleneglycol)-modified hemoglobin vesicles on agonist-induced platelet aggregation and RANTES release in vitro. *Artif Cells Blood Substit Immobil Biotechnol* **29**:191–201.

Address correspondence to: Dr. Eishun Tsuchida, Advanced Research Institute for Science and Engineering, Waseda University, Tokyo 169-8555, Japan. E-mail: eishun@waseda.jp

Exchange transfusion with entirely synthetic red-cell substitute albumin-heme into rats: Physiological responses and blood biochemical tests

Yubin Huang,[1] Teruyuki Komatsu,[1] Hisashi Yamamoto,[2] Hirohisa Horinouchi,[3] Koichi Kobayashi,[3] Eishun Tsuchida[1]

[1]*Advanced Research Institute for Science and Engineering, Waseda University,3-4-1 Okubo, Shinjuku, Tokyo 169-8555, Japan*

[2]*Pharmaceutical Research Center, NIPRO Corporation, 3023 Nojimachi, Kusatsu, Shiga 525-0055, Japan*

[3]*Department of General Thoracic Surgery, School of Medicine, Keio University,35 Shinanomachi, Shinjuku, Tokyo 160-8582, Japan*

Received 24 October 2003; revised 13 May 2004; accepted 2 June 2004
Published online 5 August 2004 in Wiley InterScience (www.interscience.wiley.com). DOI: 10.1002/jbm.a.30127

Abstract: Recombinant human serum albumin (rHSA) incorporating 2-[8-{*N*-(2-methylimidazolyl)}octanoyloxymethyl]-5,10,15,20-[tetrakis{α,α,α,α-*o*-(1-methylcyclohexanoyl)amino}-phenyl]porphinatoiron(II) [albumin-heme (rHSA-heme)] is an artificial hemoprotein which has the capability to transport O_2 *in vitro* and *in vivo*. A 20% exchange transfusion with rHSA-heme into anesthetized rats has been performed to evaluate its clinical safety by monitoring the circulation parameters and blood parameters for 6 h after the infusion. Time course changes in all parameters essentially showed the same features as those of the control group (without infusion) and rHSA group (with administration of the same amount of rHSA). Blood biochemical tests of the withdrawn plasma at 6 h after the exchange transfusion have also been carried out. No significant difference was found between the rHSA-heme and rHSA groups, suggesting the initial clinical safety of this entirely synthetic O_2-carrier as a red-cell substitute. © 2004 Wiley Periodicals, Inc. J Biomed Mater Res 71A: 63–69, 2004

Key words: exchange transfusion; entirely synthetic red-cell substitute; albumin-heme; blood biochemical tests; O_2 carrier.

INTRODUCTION

Although hemoglobin (Hb)-based O_2 carriers are currently undergoing clinical trials as red-cell substitutes or oxygen therapeutics, there are still some concerns about new infectious pathogens in Hb and unresolved side effects such as vasoconstriction.[1–4] Recombinant human serum albumin (rHSA) incorporating the synthetic heme albumin-heme is an artificial hemoprotein that has the potential to bind and release O_2 under physiological conditions in the same manner as Hb and myoglobin.[5–7] In fact, the albumin-heme can transport O_2 through the body and release O_2 to tissues as a red-cell substitute without any acute side effects.[8,9] For example, rHSA including four molecules of 2-[8-{*N*-(2-methylimidazolyl)}-octanoyloxymethyl]-5,10,15,20-[tetrakis{α,α,α,α-*o*-(1-methylcyclohexanoyl)amino}phenyl]porphinatoiron(II) (Scheme 1) is one of the promising materials.[7] Recent study on the 30% exchange transfusion with rHSA-heme after 70% hemodilution with 5 wt % rHSA with the use of anesthetized rats demonstrated that the administration of this material improved the circulatory volume and resuscitated the hemorrhagic shock state.[10] The declined MAP and the mixed venous partial O_2 pressure immediately recovered, and the lowered renal cortical O_2-pressure also significantly increased.

In order to evaluate the initial clinical safety of this albumin-based O_2-carrier, a 20% exchange transfusion with rHSA-heme into anesthetized rats was performed, and the time courses of the circulation parameters (MAP, HR, respiration rate) and blood parameters (paO_2, pvO_2, pH, blood cell numbers) were measured for 6 h, which is adequate time to determine acute toxicity. Blood biochemical tests of the withdrawn plasma were also been carried out.

MATERIALS AND METHODS

Preparation of rHSA-heme

Recombinant human serum albumin (rHSA, Albrec®, 25 wt %) was obtained from the NIPRO Corp. (Osaka). The 5

Correspondence to: E. Tsuchida; e-mail: eishun@waseda.jp
Contract grant sponsor: MHLW
Contract grant sponsor: JSPS; contract grant number: 16350093
Contract grant sponsor: MEXT; contract grant number: 16655049

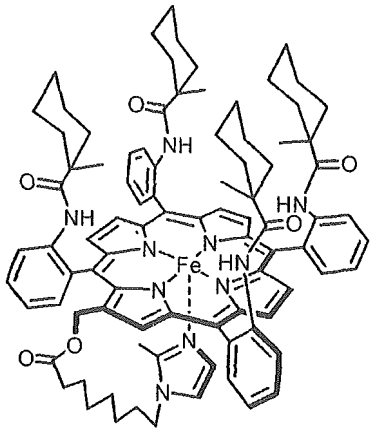

Scheme 1

g/dL rHSA was made by diluting Albrec® with saline solution (Otsuka Pharmaceutical Co., Ltd.). The rHSA-heme solution ([rHSA]: 4.9 g/dL, pH 7.45, [heme]: 2.8 m*M*, O_2-binding affinity ($p_{1/2}O_2$): 37 Torr) used for the experiments was prepared according to a previously reported procedure.[11] The red-colored rHSA-heme solution was filtered with the use of DISMIC 25CS045AS just before use.

Exchange transfusion

The investigations were carried out with 18 male Wister rats (305±3.6 g). The animals were placed on the heating pad under an inhalation anesthesia with sevofluran; its concentration was kept 2.0% for the operations and 1.5% for the experiments. After incision was made in the neck, the heparinized catheter (Natsume Seisakusho SP-55) was introduced into the right common carotid artery for blood withdrawal. Other catheters (SP-31) were inserted into the left femoral artery for a continuous MAP monitoring, and the right femoral vein for sample injection.

After stabilization of the animal condition, the 20% exchange transfusion (total blood volume of rat was estimated to be 64 mL/kg weight) was performed by 1 mL blood withdrawal via the common carotid artery and 1 mL rHSA-heme infusion from the femoral vein (each 1 mL/min) with four repeating cycles (n = 6, rHSA-heme group). Blood was taken from the artery (0.3 mL) and vein (0.2 mL) at the following five points; (i) before, (ii) immediately after, (iii) 1 h after, (iv) 3 h after, and (v) 6 h after the exchange transfusion. MAP and HR were recorded with the use of a polygraph system (NIHON KODEN LEG-1000 Ver. 01-02 or PEG-1000 Ver. 01-01) at the same time point as stated above. Withdrawn blood was rapidly applied to a blood gas system (Radio Meter Trading ABL555) to obtain the O_2-pressure (paO_2) and pH for the arterial blood, and the O_2-pressure (pvO_2) for the venous blood. The blood cell numbers were counted by a multisystem automatic blood cell counter (Sysmex KX-21). After 6 h, 4 mL of the venous blood was taken for each animal before sacrifice by sodium pentobarbital overdose. The blood samples were centrifuged at 4°C (Beckman Coulter Co., Optima LE-80K for 3500 × rpm, 10 min), and the plasma phase was frozen (−20°C) for blood biochemical tests. As a reference group, the 5 g/dL rHSA solution was administered similarly into rats (n = 6, rHSA group). Furthermore, six rats without infusion (operation only) were also set as a control group.

All animal handling and care was in accordance with the NIH guidelines. The protocol details were approved by the Animal Care and Use Committee of Keio University.

Blood biochemical tests

A total of 30 analytes, that is, total protein (TP), albumin (Alb), albumin/globulin ratio (A/G), aspartate aminotransferase (AST), alanine aminotransferase (ALT), lactate dehydrogenase (LDH), alkaline phosphatase (ALP), γ-glutamyltransferase (γ-GTP), leucine aminopeptidase (LAP), choline esterase (ChE), total bilirubin (TBil), direct bililubin (DBil), creatinine (CRN), blood urea nitrogen (BUN), uric acid (UA), amylase, lipase, creatine phosphokinase (CPK), total cholesterol (TCho), free cholesterol (FCho), cholesterol ester (ECho), β-lipoprotein (β-LP), high-density lipoprotein (HDL)-cholesterol, neutral fat (triglyceride, TG), total lipid, free fatty acid (FFA), phospholipids (PhL), K^+, Ca^{2+} and Fe^{3+}, were measured by Kyoto Microorganism Institute (Kyoto).

Data analysis

MAP, HR, respiration rate, paO_2 and pvO_2 were represented as percent ratios of the basal values with mean ± standard error of mean (SEM). Body temperature, pH, blood cell numbers and the data of blood biochemical tests were shown as mean ± SEM.

Statistical analysis were performed by repeated-analysis measures of variance (ANOVA) followed by the paired t-test for comparison with a basal value (body temperature), by the Bartlett test followed by the Tukey-Kramer multiple comparison test for pH, blood cell numbers, and the results of the blood biochemical tests, and by the Kruskal-Wallis test followed by the Tukey-Kramer multiple comparison test for more than three groups (MAP, HR, respiration rate, paO_2, and pvO_2). Values of $p < 0.05$ were considered significant. The statistical analytical software used was StatView (SAS Institute, Inc.).

RESULTS

Circulation parameters

The basal values of some measurements, the data values of which are represented by percent ratios, are summarized in Table I. There are no significant differences between the three groups (control, rHSA, and rHSA-heme groups).

The body temperature of each group was constantly

TABLE I
Basal Values of Each Group

	Control	rHSA	rHSA-heme
MAP (mmHg)	99 ± 2.8	101 ± 2.8	100 ± 6.1
HR (beats/min)	404 ± 19	435 ± 19	420 ± 13
Respiration rate (breaths/min)	66 ± 0.7	75 ± 4.0	70 ± 2.1
paO_2 (mmHg)	84.7 ± 3.1	84.9 ± 3.7	80.8 ± 2.2
pvO_2 (mmHg)	51.0 ± 1.5	45.7 ± 1.1	51.0 ± 1.7
Body weight (g)	305 ± 4.0	304 ± 2.8	305 ± 4.1

maintained within 36.9–37.4°C during the experiments [Fig. 1(a)].

The MAP time course in the control group demonstrated only a small deviation within 83.8–100.0% for 6 h. In the rHSA and rHSA-heme groups, the observed changes in MAP were almost the same as those of the control group. They ranged within 93.2–100 and 89.3–100%, respectively. It is remarkable that no vasoactive reaction was seen after the infusion of rHSA-heme [Fig. 1(b)].

The HR of the control, rHSA, and rHSA-heme groups remained unaltered for 6 h. The values of the control, rHSA, and rHSA-heme groups were in the range of 98.3–103.9, 96.9–108.8, and 85.7–100.0%, respectively [Fig. 1(c)].

The respiration rates also remained stable during the measurements. No significant difference was recognized among the three groups [Fig. 1(d)].

Blood-gas parameters

No difference in the pH changes was observed in the three groups. The pH values of the control, rHSA, and rHSA-heme groups were constant in the narrow ranges of 7.42–7.45, 7.42–7.44, and 7.42–7.44, respectively [Fig. 2(a)].

The paO_2 values of the control, rHSA, and rHSA-heme groups were also constant in the range of 100–108.1, 100–109.1, and 100–110.8%, respectively, by the end of measurements [Fig. 2(b)].

The pvO_2 of the control, rHSA and rHSA-heme groups demonstrated only small changes within 81.5–100.0, 84.9–108.4, and 81.9–100.0%, respectively [Fig. 2(c)].

Blood cell numbers

The Hct values of the control group were unchanged from 34.8–37.0% during the experiment. On the other hand, the 20% exchange transfusion with the

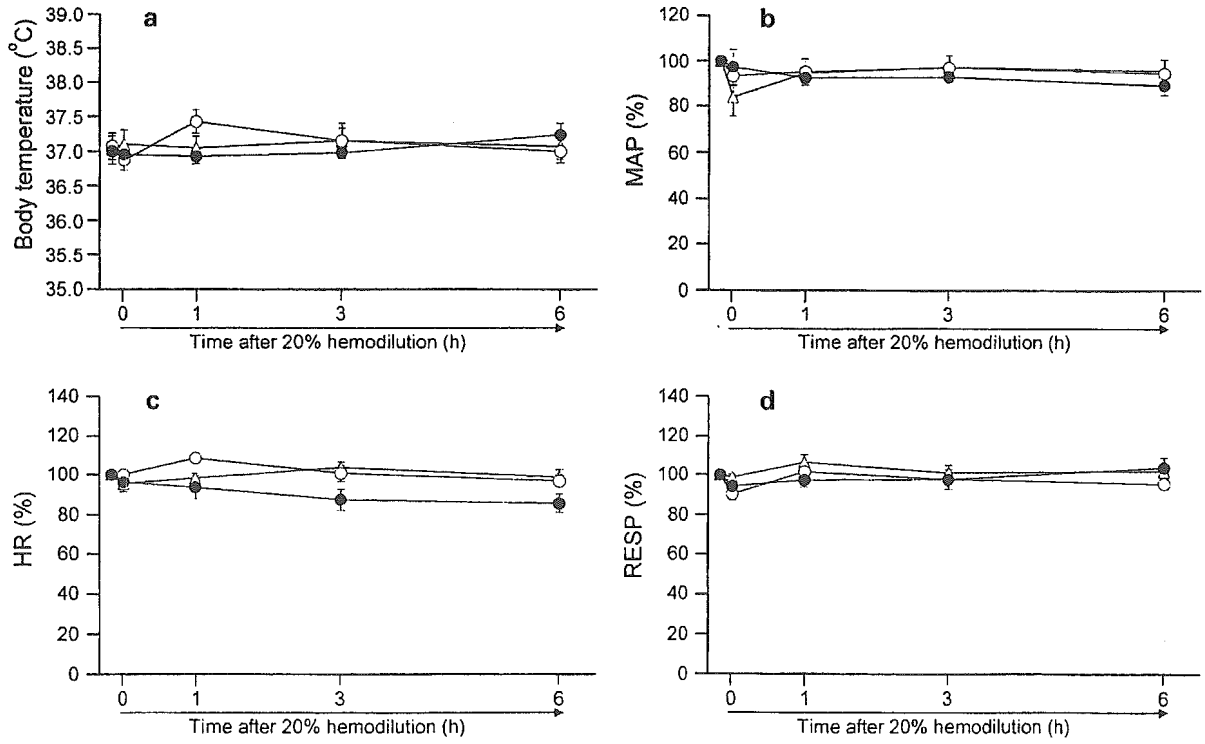

Figure 1. (a) Time courses of body temperature, (b) mean arterial pressure (MAP), (c) heart rate (HR), and (d) respiration rate (RESP) in anesthetized rats after 20% exchange transfusion with rHSA-heme or rHSA solution. Each value represents the mean ± SEM of six rats (triangles, control group without infusion; open circles, rHSA group; solid circles, rHSA-heme group).

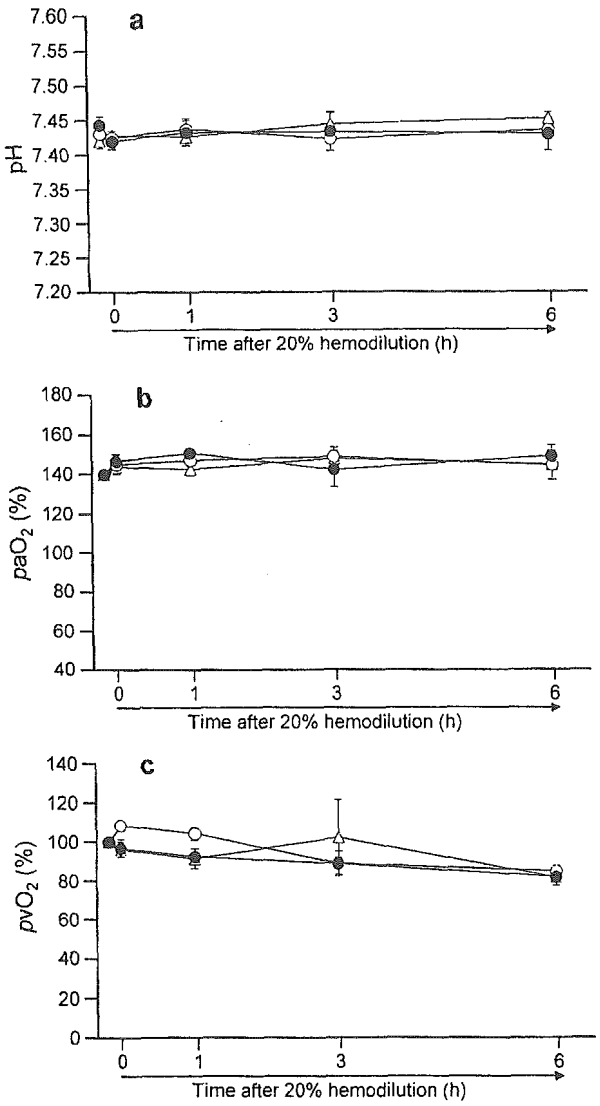

Figure 2. Time courses of (a) blood pH, (b) arterial blood O_2 pressure (paO_2), and (c) venous blood O_2-pressure (pvO_2) in anesthetized rats after 20% exchange transfusion with rHSA-heme or rHSA solution. Each value represents the mean ± SEM of six rats (triangles, control group without infusion; open circles, rHSA group; solid circles, rHSA-heme group).

rHSA or rHSA-heme solution led to rapid decreases in the Hct from 39.0 to 31.7% or from 42.2 to 33.8%, respectively. These declined values were constant for 6 h [Fig. 3(a)]. Concomitantly, the RBC numbers in the rHSA and rHSA-heme groups decreased from 634.8×10^4 to $512.8\times10^4/\mu L$ and from 620.3×10^4 to $497.7\times10^4/\mu L$ by the exchange transfusion. They did not recover for 6 h [Fig. 3(b)].

The WBC numbers in the rHSA and rHSA-heme groups also showed similar declines; however, they appeared to be relatively slow with some deviations [Fig. 3(c)]. The PLT numbers of the rHSA and rHSA-heme groups changed in the range of 57.1–76.9 × $10^4/\mu L$ and 58.4–65.6 × $10^4/\mu L$, respectively [Fig. 3(d)].

Blood biochemical tests

In order to evaluate liver function, kidney function and electrolyte balance after the infusion of rHSA-heme, total 30 analytes of the blood biochemical tests were selected for rat plasma (Fig. 4). In the rHSA group, the A/G ratio increased, and TCho, Echo, and HDL-C decreased compared to the control group.

In the rHSA-heme group, the A/G ratio and fatty acid increased, and LDH, ALP, TCho, Echo, HDL-C, and PhL decreased in comparison to the control group. However, the other analytes showed almost the same values as those of the control group. With respect to the rHSA group, no significant difference was found except for the increases in the amylase, free fatty acid, and iron concentration, and the decrease of ALP and ECho.

DISCUSSION

After the 20% exchange transfusion with the 5 g/dL rHSA solution, the Hct and RBC numbers decreased approximately 80% of their basal values. This was only because of the 20% dilution and did not imply any acute toxicity of rHSA. The significant increase in the A/G ratio was caused by the slightly high rHSA concentration of 5 g/dL. Because the albumin concentration in rat plasma is generally 3–4 g/dL, the exchange transfusion with this sample led to the increase in the albumin concentration and decrease in the globulin concentration, thus resulting in the elevated A/G ratio. The hemodilution by the 20% replacement of the animal's blood volume could reduce the level of the analytes immediately after the infusion; however, the majority of the data in the rHSA group recovered within 6 h; only LDH, TCho, Echo, and HDL-C showed values that were about 80% of the corresponding ones in the control group.

Because FCho was almost the same as that in the control group, the decreases in TCho, ECho, and HDL-C were presumably caused by the decreasing of ECho, which might come from the depressed synthetic function in the livers by administration of the external protein. The circulation parameters and blood gas parameters in the rHSA group moved within the narrow range for 6 h—almost the same as those observed in the control group. Based on these data, the authors are certain that the administration of rHSA

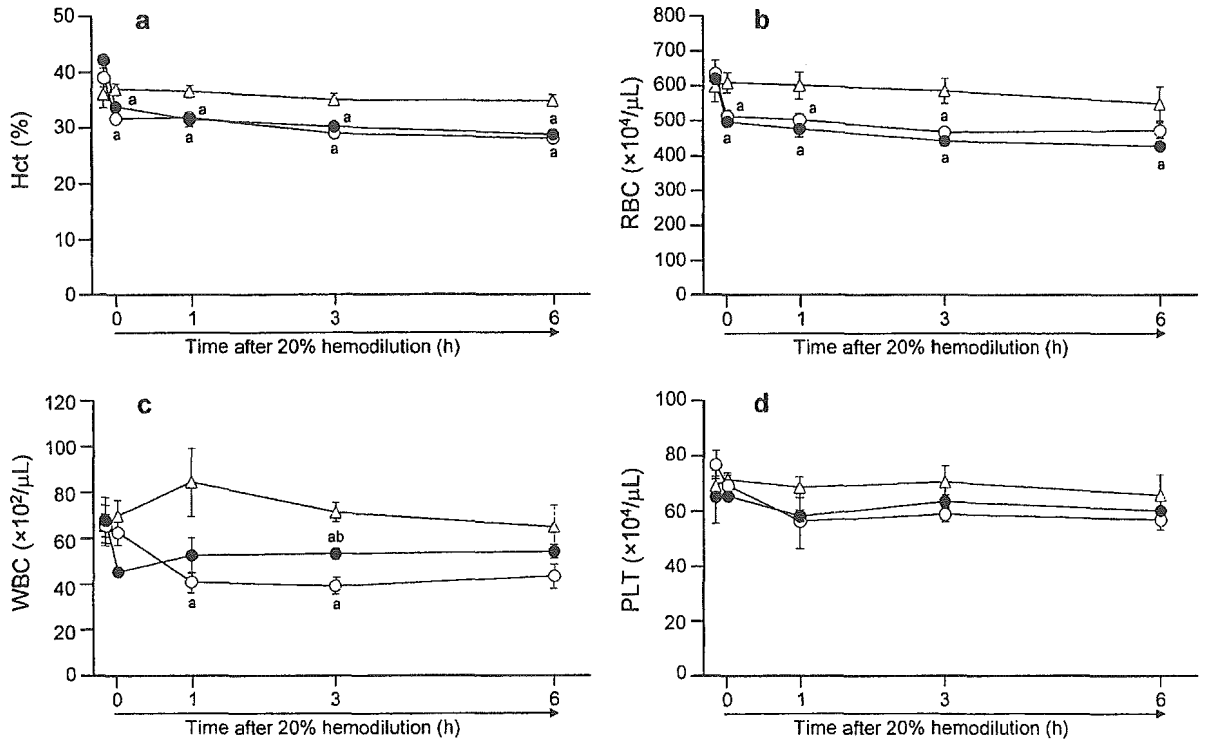

Figure 3. Time courses of hematocrit (Hct) value (a), red blood cell (RBC) numbers (b), white blood cell (WBC) numbers (c) and platelet (PLT) numbers (d) in whole blood of anesthetized rats after 20% exchange transfusion with rHSA-heme or rHSA solution. Each value represents the mean ± SEM of 6 rats (triangles, control group without infusion; open circles, rHSA group; solid circles, rHSA-heme group). $^{a}p < 0.05$ versus control group (Tukey-Kramer test).

into anesthetized rats did not induce any toxic reaction under the present experimental conditions.

After the exchange transfusion with the rHSA-heme solution, no significant difference was seen in the circulation parameters and blood gas parameters. Previous studies to elucidate the influence of albumin-heme on the MAP changes and microcirculation in the capillaries demonstrated that neither vasoconstriction nor hypertension occurred, because of the low permeability of the albumin vehicle through the vascular endothelium.[9] The latest exchange transfusion experiment with rHSA-heme after isovolemic hemodilution also supported this hypothesis.[10]

By careful inspection of the results from the blood biochemical tests, it was found that the rHSA-heme group showed higher values of amylase and free fatty acid, and lower values of ALP and ECho compared to those of the rHSA group. In general, amylase has two isozymes, which are secreted by the pancreatic parenchyma and salivary gland. When the concentrations of the amylase and lipase (pancreatic parenchyma enzyme) simultaneously increase, it may be a sign of pancreatitis and other pancreas disorders.[12–14] However, the slight increase in the lipase concentration in the current protocol was not significant. Therefore, the possibility of pancreas disorders caused by the rHSA-heme infusion is considered negligible. The high amylase value is probably due to the isozyme secreted by the salivary gland.

With the increase in the free fatty acid, the TG concentration also tended to elevate to some degree. The increase in TG may activate the lipase, which acts as its decomposition enzyme, and results in the increasing free fatty acid as a metabolite. The relation between rHSA-heme and the TG increase is still not clear.

CONCLUSIONS

The appearance of the all animals showed absolutely no change for 6 h after the 20% exchange transfusion with albumin-heme. The physiological responses of the blood circulation, gas equilibria, and blood cell numbers in the rHSA-heme group were almost the same as those of the control and rHSA groups. MAP and HR did remain constant after the injection of the rHSA-heme, suggesting again that the albumin-based O_2-carrier does not induce the vasoconstriction. The blood biochemical tests of the withdrawn plasma of rHSA-heme group showed results similar to those of the control and rHSA groups, implying no acute toxicity by the exchange transfusion

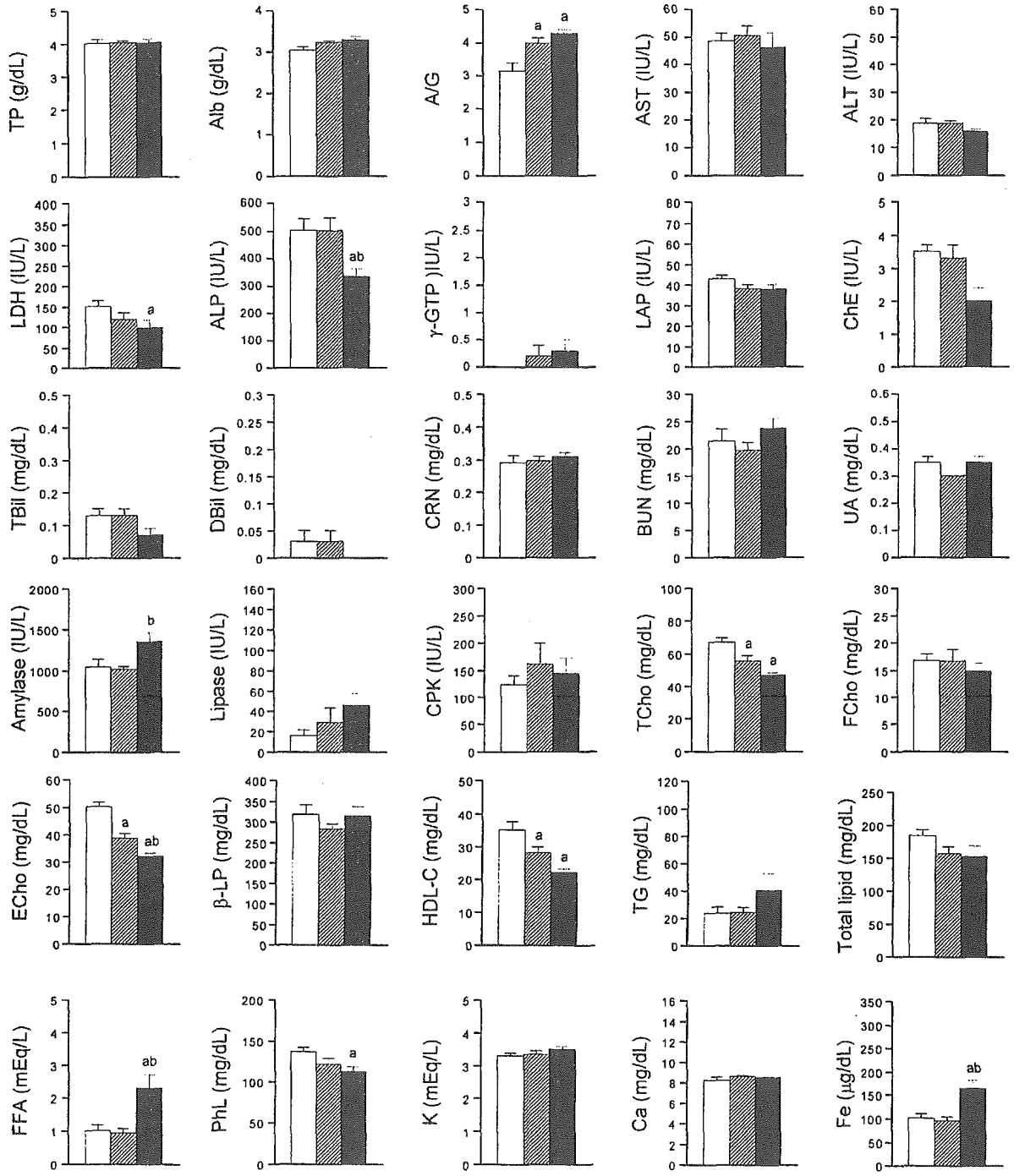

Figure 4. Blood biochemical tests of rat plasma after 20% exchange transfusion with rHSA-heme or rHSA solution. Each value represents the mean ± SEM of six rats (white bar, control group without infusion; diagonal bar, rHSA group; black bar, rHSA-heme group). [a] $p < 0.05$ versus control group (Tukey-Kramer test); [b] $p < 0.05$ versus rHSA group (Tukey-Kramer test).

with rHSA-heme. These results showed the initial clinical safety of the rHSA-heme solution, which allows us to undergo further advanced preclinical testing of this synthetic O_2-carrying hemoprotein as a new class of red-cell substitutes. Biochemical tests and histopathological observations for 7 days after the exchange transfusion with rHSA-heme will be reported in a forthcoming article.

The authors are grateful to Dr. Toshiya Kai (NIPRO Corp.) for preparation and characterizations of the albumin-heme solutions. They also thank Dr. Ichiro Hirotsu

(NIPRO Corp.) for his useful discussions and valuable suggestions on the experimental results. This work was partially supported by Health Science Research Grants (Research on Pharmaceutical and Medical Safety) of the MHLW, Grant-in-Aid for Scientific Research (No. 16350093) from JSPS, and Grant-in-Aid for Exploratory Research (No. 16655049) from MEXT.

References

1. Chang TMS. Recent and future developments in modified hemoglobin and microencapsulated hemoglobin as red blood cell substitutes. Artif Cells Blood Substit Immobil Biotechnol 1997;25:1–24.
2. Tsuchida E. Perspectives of blood substitutes. In: Tsuchida E, editor. Blood substitutes: Present and future perspectives. Lausanne: Elsevier; 1998. p 1–14.
3. Winslow RM. New transfusion strategies: red cell substitutes. Annu Rev Med 1999;50:337–353.
4. Squires JE. Artificial blood. Science 2002;295:1002–1005.
5. Komatsu T, Hamamatsu K, Wu J, Tsuchida E. Physicochemical properties and O_2-coordination structure of human serum albumin incorporating tetrakis(*o*-pivamido)phenylporphyrinatoiron(II) Derivatives. Bioconjug Chem 1999;10:82–86.
6. Tsuchida E, Komatsu T, Matsukawa Y, Hamamatsu K, Wu J. Human serum albumin incorporating tetrakis(*o*-pivalamido-)phenylporphinatoiron(II) derivative as a totally synthetic O_2-carrying hemoprotein. Bioconjug Chem 1999;10:797–802.
7. Komatsu T, Matsukawa Y, Tsuchida E. Effect of heme structure on O_2-binding properties of human serum albumin–heme hybrids: intramolecular histidine coordination provides a stable O_2-adduct complex. Bioconjug Chem 2002;13:397–402.
8. Tsuchida E, Komatsu T, Hamamatsu K, Matsukawa Y, Tajima A, Yoshizu A, Izumi Y, Kobayashi K. Exchange transfusion of albumin-heme as an artificial O_2-infusion into anesthetized rats: physiological responses, O_2-delivery and reduction of the oxidized hemin sites by red blood cells. Bioconjug Chem 2000;11:46–50.
9. Tsuchida E, Komatsu T, Matsukawa Y, Nakagawa A, Sakai H, Kobayashi K, Suematsu M. Human serum albumin incorporating synthetic heme: red blood cell substitute without hypertension by nitric oxide scavenging. J Biomed Mater Res 2003; 64A:257–261.
10. Komatsu T, Yamamoto H, Huang Y, Horinouchi H, Kobayashi K, Tsuchida E. Physiological responses to exchange transfusion with synthetic oxygen-carrier "albumin-heme" in acute anemia after 70% hemodilution. J Biomed Mater Res. Submitted for publication.
11. Huang Y, Komatsu T, Nakagawa A, Tsuchida E, Kobayashi S. Compatibility *in vitro* of albumin-heme (O_2-carrier) with blood cell components. J Biomed Mater Res 2003;66A:292–297.
12. Gorelick FS. Acute pancreatitis. In: Yamada T, editor. Textbook of gastroenterology (2nd ed.). Philadelphia: Lippincott; 1955. p 2064–2091.
13. Agarwal N, Pitchumoni CS, Sivaprasad AV. Evaluating tests for acute pancreatitis. Am J Gastroenterol 1990;85:356–361.
14. Clavin PA, Burgan S, Moossa AR. Serum enzyme and other laboratory tests in acute pancreatitis. Br J Surg 1989;76:1234–1238.

ARTICLE

OBC

www.rsc.org/obc

Synthesis of protoheme IX derivatives with a covalently linked proximal base and their human serum albumin hybrids as artificial hemoprotein

Akito Nakagawa, Naomi Ohmichi, Teruyuki Komatsu and Eishun Tsuchida*

Advanced Research Institute for Science and Engineering, Waseda University, 3-4-1 Ohkubo, Shinjuku-ku, Tokyo 169-8555, Japan. E-mail: eishun@waseda.jp; Fax: +81 3-3205-4740; Tel: +81 3-5286-3120

Received 15th June 2004, Accepted 3rd September 2004
First published as an Advance Article on the web 27th September 2004

The simple one-pot reaction of protoporphyrin IX and ω-(*N*-imidazolyl)alkylamine or *O*-methyl-L-histidyl-glycine with benzotriazol-1-yl-oxytris(dimethylamino)phosphonium hexafluorophosphate at room temperature produced a series of protoporphyrin IX species with a covalently linked proximal base at the propionate side-chain. The central iron was inserted by the general $FeCl_2$ method, converting the free-base porphyrins to the corresponding protoheme IX derivatives. Mesoporphyrin IX and diacetyldeuteroporphyrin IX analogues were also prepared by the same procedure. The Fe(II) complexes formed dioxygen (O_2) adducts in dimethylformamide at 25 °C. Some of them were incorporated into the hydrophobic domain of recombinant human serum albumin (rHSA), providing albumin–heme hybrids (rHSA–heme), which can bind and release O_2 in aqueous media (pH 7.3, 25 °C). The oxidation process of converting the dioxygenated heme in rHSA to the inactive Fe(III) state obeyed first-order kinetics, indicating that the μ-oxo dimer formation was prevented by the immobilization of heme in the albumin scaffold. The rHSA–heme, in which the histidylglycil tail coordinates to the Fe(II) center, showed the most stable O_2 adduct complexes.

Introduction

Numerous model compounds of hemoglobin (Hb) and myoglobin (Mb) have already been prepared and their O_2-binding equilibria and kinetics were extensively studied.[1] In particular, synthetic hemes having a sterically encumbered porphyrin platform can form stable O_2 adducts in organic solvent at room temperature. If we are to reproduce or mimic any biochemical reaction, the aqueous medium is particularly important. The dioxygenated complexes of highly-modified hemes are unfortunately oxidized to the ferric state in water. Human serum albumin (HSA) is the most abundant plasma protein in our circulatory system and solubilizes hydrophobic small molecules.[2] We have found that synthetic hemes are also spontaneously incorporated into HSA, which provides unique albumin–heme hybrids (HSA–hemes) and allows their Fe(II) states to remain stable in aqueous solution.[3] Actually, recombinant HSA[4] (rHSA) including tetrakis(α,α,α,α-*o*-pivalamidophenyl)porphinatoiron(II) with a covalently linked proximal base can reversibly bind and release O_2 under physiological conditions, and acts as an artificial O_2 transporter in the blood stream.[5] Our next target is to realize O_2 coordination to rHSA–heme involving protoheme IX in the same manner as natural Hb and Mb. The dioxygenation of protoheme IX has several advantages. (1) Synthetic procedures are rather simplified with respect to the highly modified tetraphenylporphyrin. (2) It has the same structure and thus the same spectra as do hemoproteins; this makes possible the study of subtle changes in the protein nanostructure. (3) Its metabolism process has been clarified,[6] which is an advantage for medical use as an artificial O_2 carrier.

We report herein the simple synthetic methodology of protoheme IX derivatives with a covalently-linked proximal imidazolyl arm and the O_2-binding properties of the obtained rHSA–hemes.

DOI: 10.1039/b409017a

Results and discussion

Synthesis

The free-base porphyrins with a covalently linked proximal base (**1a–8a**, Scheme 1) were synthesized by the one-pot reaction of protoporphyrin IX, ω-(*N*-imidazolyl)alkylamine [R_2H; 3-(*N*-imidazolyl)propylamine, 4-(*N*-(2-methylimidazolyl))-butylamine or *O*-methyl-L-histidyl-glycine] for one propionic acid group, and a capping alcohol or amine on the other side (R_3H; MeOH, EtOH or $MeNH_2$) in the presence of benzotriazol-1-yl-oxytris(dimethylamino)phosphonium hexafluorophosphate (BOP) at 25 °C in pyridine [or dimethylformamide (DMF)] (Scheme 2). The carbonyl attachment was made through either an ester or an amide function. After the reaction, the mixture was poured into 10% NaCl solution, which led to the precipitation of the crude porphyrin. Centrifugation at 7000 g for 30 min gave a purple pellet. The pyridine (or DMF), BOP, R_2H and R_3H in the supernatant were all discarded at this point. The obtained precipitate was dissolved in $CHCl_3$ and showed several spots on a thin layer chromatograph. The anpolar band corresponds to the double R_3-substituted component (ex. protoporphyrin IX diethyl ester in the cases of **2**, **5**, **6**) and the second band is the desired porphyrin, which is purified by a silica gel chromatographic separation (yield: 20–30%). The iron was then inserted by the general $FeCl_2$ method with 2,6-lutidine in DMF solution, giving the corresponding hemins. Mesoporphyrin IX and diacetyldeuteroporphyrin IX also gave similar analogues (**7b** and **8b**). We obtained a mixture of two isomeric compounds that we were unable to separate.

Traylor and co-workers reported many pioneering studies on "chelated hemes".[7] They synthesized compound **1b**, for instance, using an acid anhydride procedure directly from protohemin chloride.[7e] First, the protohemin dimethyl ester was partially hydrolyzed and, after purification, the mono acid was coupled to a 3-(*N*-imidazolyl)propylamine by the pivaloyl chloride method. Nevertheless, reaction mixtures involving the diacid and monoacid are normally insoluble in common organic solvents, therefore, the yield of this reaction largely depends on the separation techniques. In contrast, our simple procedure makes it possible to synthesize a series of new protoporphyrins with a wide variety of proximal bases and end-capping groups of the other propionic acid.

Dioxygenation of heme in DMF solution

The obtained hemin complexes **1b–8b** in DMF solution were reduced to the corresponding Fe(II) complexes using a solution

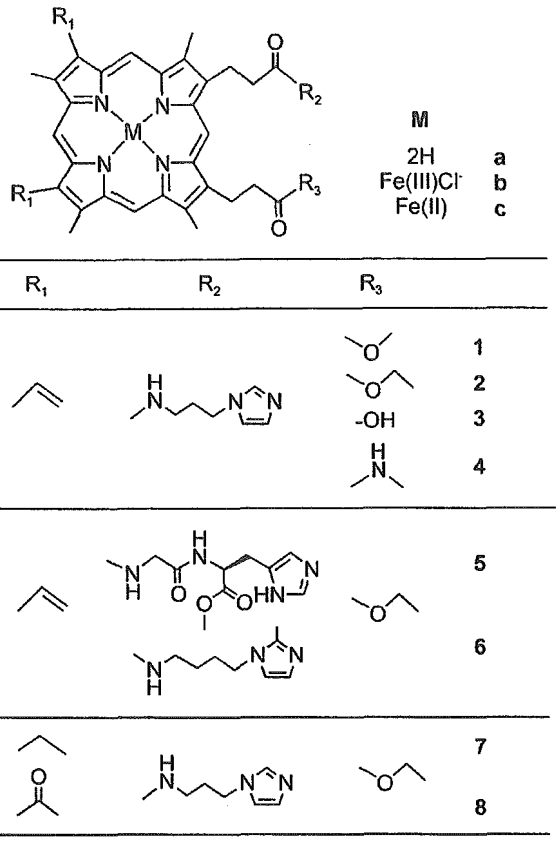

Scheme 1

of the crown ether-dithionite as reducing agent.[8] The UV-vis absorption spectrum of **2c** [Fe(II) complex] under a nitrogen (N_2) atmosphere showed a single broad band in the α,β region around 520–580 nm. This indicates the formation of a typical five-*N*-coordinate high-spin complex,[7] in which the proximal imidazole group intramolecularly coordinates to the central Fe(II) ion in the non-coordinating solvent (DMF) (Fig. 1). Because 2-methyl-imidazole significantly inhibits a sixth ligand binding to the *trans*-position, **6c** also demonstrated a similar 5-coordinated spectrum in DMF solution. Upon bubbling of the O_2 gas through the solution of **2c**, the spectral pattern immediately changed to that of the O_2 adduct complex. After adding carbon monoxide (CO) gas, the heme changed to a very stable carbonyl complex. Similar absorption changes were observed for all the heme derivatives, **1c–8c**. The absorption maxima (λ_{max}) of compounds **1c–8c** in DMF solution under N_2, O_2 and CO atmospheres are summarized in Table 1.

The positions and the relative intensities of all peaks were independent of the temperature changes from 5 to 25 °C. In general, the electron density of the porphyrin ring systematically changes the λ_{max} of the B-band and Q-band.[9] The replacement of the vinyl groups at the 3,8-positions of protoheme IX with ethyl groups (from **2c** to **7c**) produced a hypsochromic shift. In contrast, changing the vinyl groups to electron withdrawing acetyl groups (from **2c** to **8c**) produced a bathochromic shift.

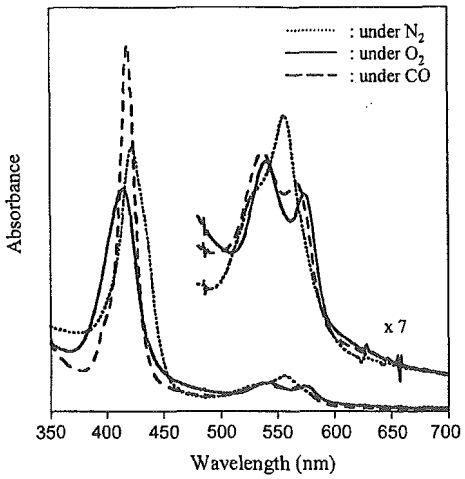

Fig. 1 UV-vis spectra of **2c** in DMF at 25 °C.

Table 1 Absorption maxima (λ_{max}) of heme derivatives in DMF under various conditions

	λ_{max}/nm		
Compound	Under N_2	Under O_2	Under CO
1c (15 °C)	427, 530, 558	414, 543, 575	420, 540, 569
1c (25 °C)	424, 532, 559	412, 542, 575	420, 539, 567
2c (5 °C)	422, 531, 556	415, 541, 574	419, 537, 567
2c (25 °C)	421, 533, 557	409, 539, 571	418, 537, 565
3c (25 °C)	426, 537, 559	415, 543, 575	420, 539, 567
4c (5 °C)	421, 527, 555	413, 540, 572	417, 536, 564
5c (5 °C)	419, 529, 551	406, 537, 569	412, 534, 562
5c (25 °C)	423, 533, 557	408, 539, 573	419, 538, 567
6c (5 °C)	430, 555	413, 547, 576	418, 538, 561
7c (25 °C)	414, 523, 548	407, 531, 563	409, 529, 556
8c (5 °C)	440, 541, 571	432, 552, 579	434, 549, 576
8c (25 °C)	439, 545, 569	431, 552, 580	433, 548, 577

We could not find any significant difference in the absorption maxima of **1c–6c**, because modification of the propionic acids did not affect the electron density of the porphyrin macrocycle.

Preparation of rHSA–heme

Aqueous solutions of rHSA–heme were prepared by injecting an ethanol solution of the carbonylated heme into an aqueous solution of rHSA. The inclusion of heme into rHSA was confirmed by the following results: (1) Sepharose gel column chromatography showed the elution peaks of heme and rHSA coincided at the same position, (2) during dialysis of the rHSA–heme solution against phosphate buffer, the outer aqueous phase did not contain the heme component. The UV-vis absorption spectra of the obtained solution showed that the heme was retained as a CO adduct complex.

The binding number of heme in one rHSA was determined to be 0.9–1.1 (mol/mol) by assaying the iron and rHSA concentrations. The binding constant of **1b** for rHSA was estimated to be *ca.* 4×10^6 M^{-1}, which is approximately 1/25 of that for protohemin IX itself to albumin (*ca.* 1×10^8 M^{-1}).[10] Polar heme derivatives **3c** with monopropionic acid and **4c** with a methyl-

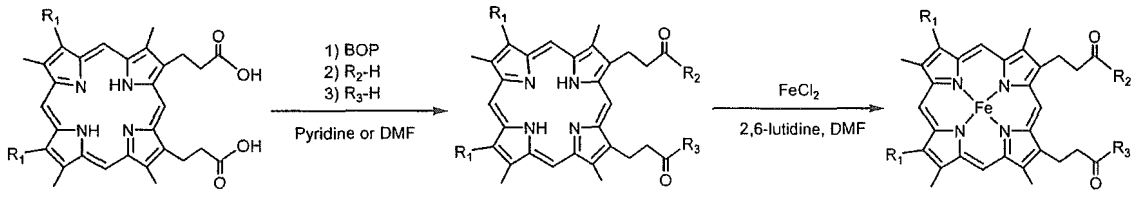

BOP: benzotriazol-1-yl-oxytris(dimethylamino)phosphonium hexafluorophosphate

Scheme 2 Synthesis of protoheme IX derivatives.

Table 2 Absorption maxima (λ_{max}) of rHSA–hemes in phosphate buffer solution (pH 7.3) at 25 °C

Compounds	λ_{max}/nm		
	Under N_2	Under O_2	Under CO
rHSA–**1c**	420, 536, 561	414, 540, 567	419, 541, 566
rHSA–**2c**	420, 538, 561	416, 540, 567	421, 543, 567
rHSA–**5c**	422, 539, 561	418, 540, 571	422, 541, 569
rHSA–**8c**	444, 549, 571	432, 551, 580	440, 555, 578

amide capping group at the porphyrin periphery were partially oxidized to the Fe(III) state during the inclusion process. Since the binding force of the heme derivative to rHSA is a hydrophobic interaction,[11] relatively polar porphyrins may not be incorporated into a certain domain of rHSA and easily oxidized compared to more apolar ones.

The circular dichroism spectra of the rHSA–hemes (rHSA–**1c**, –**2c**, –**5c**, –**7c** and –**8c**) are almost identical to that of rHSA itself (not shown). This suggests that the secondary structure of the albumin host molecule did not change after incorporation of the hemes. Furthermore, the isoelectric points of these rHSA–hemes were all 4.8, which is the original value of rHSA. The surface net charges of rHSA remained unaltered after heme incorporation.

Dioxygenation of rHSA–heme in aqueous solution

Light irradiation of the CO adduct complex of rHSA–heme (rHSA–**1c**, –**2c**, –**5c**, –**6c**, –**7c** and –**8c**) under an N_2 atmosphere led to CO dissociation and demonstrated new spectral patterns with well-defined α and β bands. For example, the typical absorption spectral changes of rHSA–**2c** are shown in Fig. 2.

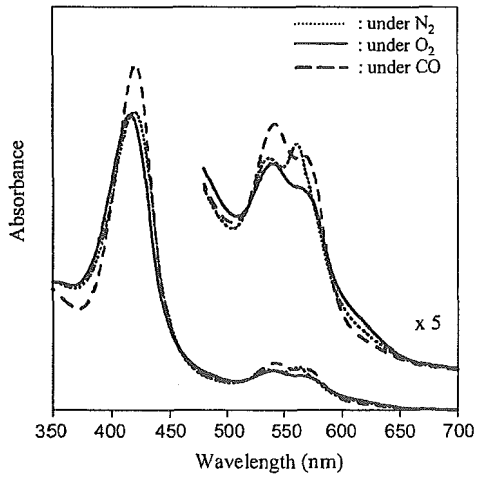

Fig. 2 UV-vis spectra of rHSA–**2c** in phosphate buffer solution (pH 7.3) at 25 °C.

From the nature of these spectra, we concluded that the obtained Fe(II) complexes are a mixture of Fe(II) 5-coordinated (high-spin) and 6-coordinated (low spin) species. It implies that the sixth coordinate position of the heme might be partially occupied by some amino acid residue of the protein scaffold. Upon exposure of O_2 to the Fe(II) complex of rHSA–**1c**, the spectrum changed to that of the O_2 adduct species. Although the aqueous micelle solution of **1c** with 5% surfactant (cetyltrimethylammonium bromide) forms a CO adduct complex, dioxygenation was not stable enough to measure the spectrum at 25 °C.[7c] In contrast, rHSA–**1c**, –**2c**, –**5c**, and –**8c** formed O_2 adduct complexes at 25 °C (pH 7.3) except for rHSA–**6c** and –**7c** (Table 2). The introduction of a methyl group to the 2-position of the imidazole ring is widely recognized to reduce the O_2 and CO binding affinities.[1] In this case, the strength of the imidazole coordination to the Fe(II) center is too weak to produce a stable O_2 adduct complex.

Table 3 Half-life ($\tau_{1/2}$) and O_2 binding affinity ($P_{1/2}$) of rHSA–hemes in phosphate buffer solution (pH 7.3) at 25 °C

Compounds	$\tau_{1/2}$/min	$P_{1/2}$/Torr
rHSA–**1c**	20	0.1
rHSA–**2c**	50	0.1
rHSA–**5c**	90	0.1
rHSA–**8c**	50	0.4

The oxidation process of dioxygenated rHSA–heme to the inactive Fe(III) state obeyed first-order kinetics. This indicates that the μ-oxo dimer formation was prevented by the immobilization of heme in the albumin structure. The half-life of the O_2 adduct complexes ($\tau_{1/2}$) and the O_2 binding affinities ($P_{1/2}$) of rHSA–hemes are summarized in Table 3. The histidylglycyl tail coordinated protoheme (**5c**) in rHSA showed the most stable O_2 adduct complex ($\tau_{1/2}$: 90 min) with respect to the imidazole bound ones. The more hydrophobic ethylpropionate (**2c**) also contributed to prolong the stability of the O_2 adduct complex relative to the methylpropionate protoheme (**1c**).

The $P_{1/2}$ values of rHSA–**1c**, –**2c** and –**5c** are 0.1 Torr at 25 °C. On the other hand, rHSA–**8c** showed a higher $P_{1/2}$ value (low O_2-binding affinity) compared to the others. The acetyl groups at the 3,8-positions of **8c** decrease the electron density of the porphyrin macrocycle, therefore $P_{1/2}$ could be significantly reduced. Traylor and co-workers found that the O_2 binding affinity of the chelated heme was sensitive to the electron density at Fe(II) and thus to the substituents at the heme periphery. The O_2 binding constant decreased by 1/6 upon changing the substituent from a vinyl to an acetyl group.[12] Our experimental data of hemes in rHSA are quite consistent with their observations.

Conclusion

A convenient one-pot synthesis of protoporphyrin IX derivatives with a covalently linked proximal base has been described. rHSA successfully incorporates the protoheme derivatives, providing an artificial hemoprotein, which can form an O_2 adduct complex at 25 °C. The rHSA–heme, in which the histidylglycil tail intramolecularly coordinates to the Fe(II) center, showed the most stable O_2 adduct complex with the relatively high O_2 binding affinity of 0.1 Torr.

Experimental

Materials and apparatus

All reagents were used as supplied commercially unless otherwise noted. All solvents were normally purified by distillation before use. DMF was distilled under reduced pressure in N_2. Pyridine was refluxed over and distilled from P_2O_5. The water was deionized using an ADVANTEC GS-200 system. The rHSA (Albrec®, 25 wt%) was obtained from NIPRO Corp. (Osaka).

Thin-layer chromatography was carried out on 0.2 mm precoated plates of silica gel 60 F254 (Merck). Purification was performed by silica gel 60 (Merck) column chromatography. The infrared spectra were measured with a JASCO FT/IR-410 spectrometer. The UV-vis absorption spectra were recorded by a JASCO V-570 spectrophotometer. The ^{1}H-NMR spectra were recorded using a JEOL Lambda 500 spectrometer. Chemical shifts were expressed in parts per million downfield from Me_4Si as the internal standard. The FAB-MS spectra were obtained using a JEOL JMS-SX102A spectrometer.

Synthesis of porphyrin derivatives

O-Methyl-L-histidyl-glycine[13] and 4-(*N*-(2-methylimidazolyl))-butylamine[14] were synthesized according to the reported procedures.

3,18-Divinyl-8-(3-methoxycarbonyl)ethyl-12-(3-(*N*-imidazolyl)propylamido)ethyl-2,7,13,17-tetramethylporphyrin (1a). A pyridine (7 mL) solution of 3-(*N*-imidazolyl)propylamine (35 μL, 0.29 mmol) was added dropwise to protoporphyrin IX (200 mg, 0.36 mmol) and benzotriazol-1-yloxytris-(dimethylamino)phosphonium hexafluorophosphate (411 mg, 0.93 mmol) in pyridine (20 mL) and stirred for 30 min at room temperature. The mixture was reacted for 4 h at 40 °C. After the addition of methanol (10 mL), the solution was stirred for another 12 h at 40 °C. The mixture was then poured into a 10% NaCl solution (1 L, 4 °C) and the suspension was centrifuged for 30 min at 7000*g*. The supernatant was discarded and the precipitate was collected and dried *in vacuo*. The residue was chromatographed on a silica gel column using $CHCl_3/CH_3OH$ = 8/1 (v/v) as the eluent. The main band was collected and dried at room temperature for several hours *in vacuo*, giving compound **1a** as a purple solid (75 mg, 20%). R_f = 0.3 ($CHCl_3/CH_3OH$ = 8/1 (v/v)); IR (NaCl) ν = 1731 (C=O, ester), 1646 (C=O, amide) cm^{-1}; UV-vis ($CHCl_3$) λ_{max} = 408, 506, 542, 575, 630 nm; ^{1}H-NMR ($CDCl_3$) δ: −4.0 (s, 2H, inner), 1.8–2.4 (m, 4H, –(CH_2)$_2$–Im), 2.7 (m, 4H, –CH_2–COO–, NH–CH_2–), 3.2 (t, 2H, –CONH–CH_2–), 3.3–3.7 (m, 18H, por–CH_3, –CH_2–CO–, –$COOCH_3$), 4.2 (d, 4H, por–CH_2–), 5.4 (s, 1H, Im), 6.0–6.3 (m, 4H, =CH_2 (vinyl)), 6.4 (d, 1H, Im), 6.6 (d, 1H, Im), 8.0–8.4 (m, 2H, –CH= (vinyl)), 9.7 (m, 4H, *meso*); MS *m/z*: 681.67.

Fe(III) complex of 1a (1b). Iron(II) chloride tetrahydrate (106 mg, 0.53 mmol) was added to a dry DMF (10 mL) solution of **1a** (36 mg, 53 μmol) and 2,6-lutidine (30 μL, 0.27 mmol) under an N_2 atmosphere. The reaction mixture was stirred at 70 °C for 3 h. After confirming the disappearance of the porphyrin's fluorescence (600–800 nm, ex. 400 nm), the solution was cooled to room temperature and poured into 10% NaCl solution (1 L, 4 °C). The suspension was centrifuged for 30 min at 7000*g* and the supernatant was discarded. The precipitate was dried *in vacuo* and chromatographed on a silica gel column using $CHCl_3/CH_3OH$ = 8/1 (v/v) as the eluent. The main band was collected and dried at room temperature for several hours *in vacuo* to give compound **1b** as a brown solid (27 mg, 68%). R_f = 0.3 ($CHCl_3/CH_3OH$ = 8/1); IR (NaCl) ν = 1728 (C=O, ester), 1646 (C=O, amide) cm^{-1}; UV-vis ($CHCl_3$) λ_{max} = 389, 513, 641 nm; HR-MS *m/z*: calcd for $C_{41}H_{43}O_3N_7Fe$: 737.2777, found: 737.2778 [M^+].

3,18-Divinyl-8-(3-ethoxycarbonyl)ethyl-12-(3-(*N*-imidazolyl)-propylamido)ethyl-2,7,13,17-tetramethylporphyrin (2a). The synthetic procedure of compound **2a** was the same as that used for **1a** except for using ethanol instead of methanol. Yield 30%; R_f = 0.4 ($CHCl_3/CH_3OH$ = 10/1); IR (NaCl) ν = 1650 (C=O, amide), 1732 (C=O, ester) cm^{-1}; UV-vis ($CHCl_3$) λ_{max} = 409, 544, 580, 633 nm; ^{1}H-NMR ($CDCl_3$) δ: −4.1 (s, 2H, inner-NH), 0.8–0.9 (t, 3H, –COO–CH_2–CH_3), 1.3–1.5 (t, 2H, –CONH–CH_2–CH_2–), 3.0–3.1 (t, 2H, –CH_2–Im), 3.1–3.3 (m, 4H, –CH_2–COO), 3.5–3.7 (m, 12H, por–CH_3), 3.8–3.9 (m, 2H, –COO–CH_2–CH_3), 4.2–4.4 (d, 4H, por–CH_2–), 6.1 (s, 1H, Im), 6.1–6.4 (q, 5H, =CH_2 (vinyl), Im), 6.6–6.7 (d, 1H, Im), 6.9–7.0 (d, 1H, Im), 8.1–8.3 (m, 2H, –CH= (vinyl)), 9.8–10.2 (m, 4H, *meso*); MS *m/z*: 695.29.

Fe(III) complex of 2a (2b). Iron insertion to **2a** was carried out by the same procedure as in the **1b** preparation. Yield 80%; R_f = 0.3 ($CHCl_3/CH_3OH$ = 8/1); IR (NaCl) ν = 1651 (C=O, amide), 1725 (C=O, ester) cm^{-1}, UV-vis ($CHCl_3$) λ_{max} = 406, 520, 578 nm; HR-MS *m/z*: calcd. for $C_{42}H_{45}O_3N_7Fe$: 751.2933, found: 751.2953 [M^+].

3,18-Divinyl-8-(3-carboxy)ethyl-12-(3-(*N*-imidazolyl)propyl-amido)ethyl-2,7,13,17-tetramethylporphyrin (3a). Sodium hydroxide (2 N, 4.5 mL) was added to the methanol (10 mL) solution of **2a** (266 mg, 0.38 mmol) and the mixture was stirred for 12 h at room temperature. It was brought to dryness *in vacuo*. Methanol was added to the residue and the mixture was added dropwise to 10% NaCl solution (pH 2, 4 °C). It was centrifuged for 30 min at 7000*g* and the precipitate was collected and dried *in vacuo*, affording compound **3a** as a brown solid (187 mg, 78%), IR (KBr) ν = 1652 (C=O, amide), 1707 (C=O, –COOH) cm^{-1}; UV-vis (DMSO) λ_{max} = 409, 508, 543, 578, 631 nm; ^{1}H-NMR (d_6-DMSO) δ: −3.5 (s, 2H, inner-NH), 1.6–1.7 (t, 2H, –CONH–CH_2–CH_2–), 2.8–2.9 (t, 2H, –CH_2–Im), 3.1–3.3 (m, 2H, –CONH–CH_2–), 3.5–3.9 (m, 12H, por–CH_3), 4.2–4.4 (d, 4H, por–CH_2–), 6.1 (s, 1H, Im), 6.1–6.4 (q, 5H, =CH_2 (vinyl), Im), 6.6–6.7 (d, 1H, Im), 6.9–7.0 (d, 1H, Im), 8.5–8.6 (m, 2H, –CH= (vinyl)), 10.2–10.4 (m, 4H, *meso*); MS *m/z*: 670.41.

Fe(III) complex of 3a (3b). Iron insertion to **3a** was carried out by the same procedure as in the **1b** preparation. Yield 80%; IR (KBr) ν = 1646 (C=O, amide), 1707 (C=O, –COOH) cm^{-1}; UV-vis (DMSO) λ_{max} = 403, 508, 631 nm; HR-MS *m/z*: calcd. for $C_{40}H_{41}O_3N_7Fe$: 723.2620, found: 724.2668 [M + H^+].

3,18-Divinyl-8-(3-methylamido)ethyl-12-(3-(*N*-imidazolyl)-propylamido)ethyl-2,7,13,17-tetramethylporphyrin (4a). Compound **4a** was synthesized according to the same procedure as for **1a** except for using methyl amine instead of methanol. Yield 20%; R_f = 0.5 ($CHCl_3/CH_3OH$ = 3/1); IR (NaCl) ν = 1631 (C=O, amide) cm^{-1}; UV-vis ($CHCl_3$) λ_{max} = 409, 509, 543, 579, 632 nm; ^{1}H-NMR (CD_3OD, $CDCl_3$) δ: −4.0 (s, 2H, inner), 1.8–2.4 (m, 4H, –(CH_2)$_2$–Im), 2.5 (t, 3H, –CONH–CH_3), 2.9 (m, 2H, –CONH–CH_2–), 3.3 (m, 4H, –CH_2–CONH–), 3.4–3.6 (m,12H, por–CH_3), 5.5 (s, 1H, Im), 6.0 (s, 1H, Im), 6.1–6.4 (m, 4H, =CH_2 (vinyl)), 6.8 (m, 1H, Im), 8.1–8.3 (m, 2H, –CH= (vinyl)), 9.7–9.9 (q, 4H, *meso*); MS *m/z*: 680.69.

Fe(III) complex of 4a (4b). Iron insertion to **4a** was carried out by the same procedure as in the **1b** preparation. Yield 67%; R_f = 0.3 ($CHCl_3/CH_3OH$ = 5/1); IR (NaCl) ν = 1646 (C=O, amide) cm^{-1}; UV-vis ($CHCl_3$) λ_{max} = 408, 521, 565 nm; HR-MS *m/z*: calcd. for $C_{41}H_{44}O_3N_7Fe$: 736.2937, found: 736.2938 [M^+].

3,18-Divinyl-8-(3-ethoxycarbonyl)ethyl-12-(((3-*N*-glycyl-L-histidinyl)-9-oxymethyl)carbonyl)ethyl-2,7,13,17-tetramethyl-porphyrin (5a). The synthetic procedure of compound **5a** was same as that used for **1a**. DMF was used instead of pyridine, because it dissolves *O*-methyl-L-histidyl-glycine. Yield 15%; R_f = 0.4 ($CHCl_3/CH_3OH$ = 15/1); IR (NaCl) ν = 1635 (C=O, amide), 1725 (C=O, ester) cm^{-1}; UV-vis ($CHCl_3$) λ_{max} = 405, 505, 541, 577, 627 nm; ^{1}H-NMR ($CDCl_3$) δ: −4.6 (s, 2H, inner-NH), 2.7–2.9 (m, 2H, Im–CH_2–), 3.0–3.5 (m, 18H, por–CH_3, –CH_2–CH_2–CO–NH–, –CH_2–CH_2–COO–CH_2–CH_3), 3.6 (s, 2H, –CONH–CH_2–CONH–), 3.8 (s, 3H,–OCH_3), 4.0–4.3 (d, 4H, por–CH_2–), 4.3–4.5 (m, 1H, α-CH), 6.0–6.4 (m, 4H, =CH_2 (vinyl)), 7.4 (s, 1H, Im–H), 8.0–8.3 (m, 5H, –CH= (vinyl), Im–H), 9.8–10.0 (m, 4H, *meso*-H); MS *m/z*: 782.68.

Fe(III) complex of 5a (5b). Iron insertion to **5a** was carried out by the same procedure as in the **1b** preparation. Yield 75%; R_f = 0.5 ($CHCl_3/CH_3OH$ = 8/1); IR (NaCl) ν = 1660 (C=O, amide), 1734 (C=O, ester) cm^{-1}; UV-vis ($CHCl_3$) λ_{max} = 388, 508, 637 nm; HR-MS *m/z*: calcd. for $C_{44}H_{46}O_6N_8Fe$: 838.2890, found: 839.2929 [M + H^+].

3,18-Divinyl-8-(3-ethoxycarbonyl)ethyl-12-(4-(*N*-(2-methyl-imidazolyl))butylamido)ethyl-2,7,13,17-tetramethylporphyrin (6a). Compound **6a** was synthesized by the same procedure as for **1a** except for using 4-(*N*-(2-methylimidazolyl))butylamine instead of 3-imidazolylpropylamine. Yield 20%; R_f: 0.1 ($CHCl_3/CH_3OH$ = 8/1); IR (NaCl) ν = 1732 (C=O, ester), 1651 (C=O, amide) cm^{-1}; UV-vis ($CHCl_3$) λ_{max} = 408, 506, 542, 576, 630 nm; ^{1}H-NMR ($CDCl_3$) δ: −4.2 (s, 2H, inner-H), 0.4–0.6 (m, 4H, CONH–CH_2–(CH_2)$_2$–), 1.4–1.5 (d, 3H, Im–CH_3), 2.2–2.4 (m,

2H, –CONH–CH_2–), 2.8–3.1 (m, 4H, por–CH_2–CH_2–), 3.2–3.3 (t, 2H, –CH_2–Im), 3.4 (s, 3H, –COO–CH_3), 3.5–3.8 (m, 12H, por–CH_3), 4.2–4.4 (t, 4H, por–CH_2–), 5.6–5.7 (d, 1H, Im), 5.8 (m, 1H, Im), 6.1–6.4 (q, 4H, =CH_2 (vinyl)), 8.1–8.2 (m, 2H, –CH= (vinyl)), 9.8–10.1 (m, 4H, *meso*); MS *m/z*: 709.72.

Fe(III) complex of 6a (6b). Iron insertion to **6a** was carried out by the same procedure as in the **1b** preparation. Yield 64%; R_f = 0.2 ($CHCl_3$/CH_3OH = 8/1); IR (NaCl) ν = 1732 (C=O, ester), 1652 (C=O, amide) cm^{-1}; UV-vis ($CHCl_3$) λ_{max} = 401, 580, 630 nm; HR-MS *m/z*: calcd. for $C_{43}H_{47}O_3N_7Fe$: 765.3090, found: 766.3184 [M + H^+].

3,18-Diethyl-8-(3-carboxy)ethyl-12-(3-(*N*-imidazolyl)propyl-amido)ethyl-2,7,13,17-tetramethylporphyrin (7a). Compound **7a** was synthesized by the same procedure as for **1a** except for using mesoporphyrin IX instead of protoporphyrin IX. Yield 10%; R_f: 0.4 ($CHCl_3$/CH_3OH = 20/1); IR (NaCl) ν = 1732 (C=O, ester), 1651 (C=O, amide) cm^{-1}; UV-vis ($CHCl_3$) λ_{max} = 408, 506, 542, 576, 630 nm; ^{1}H-NMR ($CDCl_3$) δ: 0.8 (m, 3H, CH_3–CH_2–O–), 1.6 (m, 2H,–CH_2–CH_2–Im), 1.8 (t, 6H, CH_3–CH_2–Por), 2.9 (m, 2H, CH_3–CH_2–O–), 3.1 (m, 4H, –CH_2–COO–), 3.2 (m, 2H, –NH–CH_2–), 3.6 (m, 12H, CH_3–Por), 3.8 (m, 2H,–CH_2–Im), 4.1 (m, 4H,CH_3–CH_2–Por), 4.4 (m, 4H, Por–CH_2–), 6.6 (s, 1H, –NHCO–), 6.0–6.8 (d, 3H, Im), 10.0 (m, 4H, *meso*); MS *m/z*: 699.32.

Fe(III) complex of 7a (7b). Iron insertion to **7a** was carried out by the same procedure as in the **1b** preparation. Yield 62%; R_f: 0.2 ($CHCl_3$/CH_3OH = 6/1); IR (NaCl) ν = 1732 (C=O, ester), 1668 (C=O, amide) cm^{-1}; UV-vis (DMF) λ_{max} = 394, 566, 591 nm; MS *m/z*: calcd for $C_{42}H_{49}O_3N_7Fe$: 755.3292, found 755.3246 [M^+].

3,18-Diacetyl-8-(3-carboxy)ethyl-12-(3-(*N*-imidazolyl)propyl-amido)ethyl-2,7,13,17-tetramethylporphyrin (8a). Compound **8a** was synthesized by the same procedure as for **1a** except for using diacetyldeuteroporphyrin IX instead of protoporphyrin IX. Yield 27%; R_f: 0.1 ($CHCl_3$/CH_3OH = 6/1); IR (NaCl) ν = 1735 (C=O, ester), 1651 (C=O, amide, ketone) cm^{-1}; UV-vis ($CHCl_3$) λ_{max} = 423, 516, 551, 586, 640 nm; ^{1}H-NMR ($CDCl_3$) δ: 1.5 (m, 2H, –CH_2–CH_2–Im), 2.9–3.1 (M, 4H, –CH_2–Im, –NH–CH_2–), 3.2–3.3 (m, 16H, –CH_2–COO, CH_3–Por), 3.4 (m, 6H, CH_3–CO–), 3.6 (m, 3H, CH_3–OCO–), 4.1 (m, 4H, Por–CH_2–), 6.0 (d, 1H, Im), 6.6 (m, 1H, Im), 6.9 (m, 1H, Im), 10 (m, 4H, *meso*); MS *m/z*: 712.

Fe(III) complex of 8a (8b). Iron insertion to **8a** was carried out by the same procedure as in the **1b** preparation. Yield 64%; R_f: 0.1 ($CHCl_3$/CH_3OH = 6/1); IR (NaCl) ν = 1735 (C=O, ester), 1651 (C=O, amide, ketone) cm^{-1}; UV-vis (DMF) λ_{max} = 418, 550, 578 nm; HR-MS *m/z*: calcd. for $C_{41}H_{43}O_5N_7Fe$: 769.2675, found 769.2697 [M^+].

Preparation of ferrous complex in DMF solution

The central Fe(III) ion of the porphyrin derivatives were reduced to the Fe(II) state using the complex of 18-crown-6 ether with $Na_2S_2O_4$ in DMF under aerobic conditions as previously reported.[8]

Preparation of rHSA–heme

Aqueous ascorbic acid (0.2 M, 10 μL) was added to an ethanol solution of the hemin derivative (2 mM, 1 mL) under a CO atmosphere. After complete reduction of the central Fe(III) ion, the ethanol solution (2 mM, 25 μL) was injected into the phosphate buffer solution (1 mM, pH 7.3, 2.5 mL) of rHSA (20 μM) under an Ar atmosphere. The formation of carbonyl rHSA–heme was confirmed by its UV-vis spectrum. The binding ratio of heme to rHSA was estimated by each concentration. The heme concentration was measured by the assay of iron ion using inductively coupled plasma spectrometry (Seiko, SPS7000A). The rHSA concentration was determined by bromocresol green along with the Albumin Test Wako kit (Wako Pure Chemical Industries).

Measurement of O_2 binding ability

The half-life of the O_2 adduct complex was determined by the time course of spectral changes, and the O_2 binding affinity ($P_{1/2}$) was determined by spectral changes at various partial pressures of O_2 according to previous reports.[2,15] rHSA–heme concentrations of 20 μM were normally used for UV-vis absorption spectroscopy. The spectra were recorded within the range of 350–700 nm.

Acknowledgements

This work was partially supported by a Grant-in-Aid for Scientific Research (No. 16350093) from JSPS, a Grant-in-Aid for Exploratory Research (No. 16655049) from MEXT Japan, and Health Science Research Grants from MHLW Japan.

References

1 (*a*) J. P. Collman, R. Boulatov, C. J. Sunderland and L. Fu, *Chem. Rev.*, 2004, **104**, 561; (*b*) M. Momenteau and C. A. Reed, *Chem. Rev.*, 1994, **94**, 659, and references therein.
2 T. Peters, Jr., *All about Albumin, Biochemistry, Genetics, and Medical Applications*, Academic Press, New York, 1996.
3 (*a*) T. Komatsu, K. Ando, N. Kawai, H. Nishide and E. Tsuchida, *Chem. Lett.*, 1995, 812; (*b*) T. Komatsu, K. Hamamatsu, J. Wu and E. Tsuchida, *Bioconjugate Chem.*, 1999, **10**, 82; (*c*) E. Tsuchida, T. Komatsu, Y. Mastukawa, K. Hamamatsu and J. Wu, *Bioconjugate Chem.*, 1999, **10**, 797; (*d*) T. Komatsu, T. Okada, M. Moritake and E. Tsuchida, *Bull. Chem. Soc. Jpn.*, 2001, **74**, 1695; (*e*) T. Komatsu, Y. Matsukawa and E. Tsuchida, *Bioconjugate Chem.*, 2002, **13**, 397; (*f*) A. Nakagawa, T. Komatsu, N. Ohmichi and E. Tsuchida, *Chem. Lett.*, 2003, **32**, 504.
4 A. Sumi, W. Ohtani, K. Kobayashi, T. Ohmura, K. Tokoyama, M. Nishida and T. Suyama, *Biotechnol. Blood Proteins*, 1993, **227**, 293.
5 (*a*) E. Tsuchida, T. Komatsu, Y. Matsukawa, A. Nakagawa, H. Sakai, K. Kobayashi and M. Suematsu, *J. Biomed. Mater. Res.*, 2003, **64A**, 257; (*b*) Y. Huang, T. Komatsu, A. Nakagawa, E. Tsuchida and S. Kobayashi, *J. Biomed. Mater. Res.*, 2003, **66A**, 292; (*c*) E. Tsuchida, T. Komatsu, K. Hamamatsu, Y. Matsukawa, A. Tajima, A. Yoshizu, Y. Izumi and K. Kobayashi, *Bioconjugate Chem.*, 2000, **11**, 46.
6 (*a*) P. R. Oritz de Montellano, *Curr. Opin. Chem. Biol.*, 2000, **4**, 221; (*b*) R. B. Frydman and B. Frydman, *Acc. Chem. Res.*, 1987, **20**, 250.
7 (*a*) C. K. Chang and T. G. Traylor, *J. Am. Chem. Soc.*, 1973, **95**, 8475; (*b*) C. K. Chang and T. G. Traylor, *J. Am. Chem. Soc.*, 1973, **95**, 8477; (*c*) C. K. Chang and T. G. Traylor, *Proc. Natl. Acad. Sci. USA*, 1975, **72**, 1975; (*d*) T. G. Traylor, C. K. Chang, J. Geibel, A. Berzinis, T. Mincey and J. Cannon, *J. Am. Chem. Soc.*, 1979, **101**, 6716; (*e*) J. Geibel, J. Cannon, D. Cambell and T. G. Traylor, *J. Am. Chem. Soc.*, 1978, **100**, 3575.
8 T. Mincey and T. G. Traylor, *Bioinorg. Chem.*, 1978, **9**, 409.
9 (*a*) *Porphyrins and Metalloporphyrins*, ed. K. M. Smith, Elsevier, Amsterdam, 1975; (*b*) M. Brunori, U. Saggese, G. C. Rotilio, E. Antonini and J. Wyman, *Biochemistry*, 1971, **10**, 1604.
10 G. H. Beaven, S.-H. Chen, A. D'albis and W. B. Gratzer, *Eur. J. Biochem.*, 1974, **41**, 539.
11 M. Rotenberg, S. Cohen and R. Margalit, *Photochem. Photobiol.*, 1987, **46**, 689.
12 T. G. Traylor, D. K. White, D. W. Cambell and A. P. Berzinis, *J. Am. Chem. Soc.*, 1982, **103**, 4932.
13 E. Monzani, L. Linati, L. Casella, L. D. Gioia, M. Favretto, M. Gullotti and F. Chillemi, *Inorg. Chim. Acta*, 1998, **273**, 339.
14 (*a*) E. Tsuchida, H. Nishide, Y. Sato and M. Kaneda, *Bull. Chem. Soc. Jpn.*, 1982, **55**, 1890; (*b*) K. Soai, A. Ookawa and K. Kato, *Bull. Chem. Soc. Jpn.*, 1982, **55**, 1671.
15 J. P. Collman, J. I. Brauman, B. L. Iverson, J. L. Sessler, R. M. Morris and Q. H. Gibson, *J. Am. Chem. Soc.*, 1983, **105**, 3052.

J|A|C|S
COMMUNICATIONS

Published on Web 10/19/2004

Dioxygenation of Human Serum Albumin Having a Prosthetic Heme Group in a Tailor-Made Heme Pocket

Teruyuki Komatsu,*,† Naomi Ohmichi,† Patricia A. Zunszain,‡ Stephen Curry,‡ and Eishun Tsuchida*,†

Advanced Research Institute for Science and Engineering, Waseda University, 3-4-1 Okubo, Shinjuku-ku, Tokyo 169-8555, Japan, and Department of Biological Sciences, Imperial College London, Huxley Building, South Kensington Campus, London SW7 2AZ, United Kingdom

Received July 4, 2004; E-mail: eishun@waseda.jp

Human serum albumin (HSA, MW = 66.5 kD) is the most abundant plasma protein in our bloodstream and serves as a transporter for small hydrophobic molecules such as fatty acids, bilirubin, and steroids.[1,2] Hemin dissociated from methemoglobin is also bound within a narrow D-shaped cavity in subdomain IB of HSA with an axial coordination of Tyr-161 and electrostatic interactions between the porphyrin propionates and a triad of basic amino acid residues (Figure 1).[3,4] In terms of the general hydrophobicity of the α-helical pocket, HSA potentially has features similar to the heme-binding site of myoglobin (Mb) or hemoglobin (Hb). However, even if one reduces the ferric HSA−hemin to obtain a ferrous complex, it is immediately oxidized by O_2. This is due to the fact that HSA lacks a proximal histidine, which enables the heme group to bind O_2.[3−5] We have shown that HSA incorporating tetraphenylporphinatoiron derivatives having a covalently linked axial-base can absorb O_2 under physiological conditions with a O_2 binding affinity similar to that of Hb.[6]

In this paper, we report for the first time the introduction of a proximal histidine into the subdomain IB of HSA by site-directed mutagenesis to construct a tailor-made heme pocket, which allows a reversible O_2 binding to the prosthetic heme group. Laser flash photolysis experiments revealed that this artificial hemoprotein appears to have two different geometries of the axial-imidazole coordination and shows rather low O_2 binding affinity.

We designed two recombinant HSA (rHSA) mutants, in which single or double mutations were introduced into subdomain IB: I142H [rHSA(A)] and I142H/Y161L [rHSA(B)] (Figure 1). Replacement of Y161 by histidine was not done because modeling experiments indicated that the distance from N_ϵ(H142) to Fe(heme) would be too great (>4 Å). In our mutants, the N_ϵ(H142)−Fe distance was estimated to be 2.31 Å (compared to 2.18 Å in Mb). The specific mutations were introduced into the HSA coding region in a plasmid vector (pHIL-D2 HSA) using the QuikChange (Stratagene) mutagenesis kit, and the mutants were expressed in the yeast species *Pichia pastoris*.[7] The rHSA(wild-type or mutants)−hemin complexes were prepared essentially according to our previously reported procedures, except that myristate was not added.[4] The resulting hemoproteins exhibited only a single band in SDS-PAGE.

In the absorption spectrum of the rHSA(wt)−hemin solution, the distinct charge-transfer (CT) band of Fe^{3+}−phenolate appeared at 625 nm.[8] A magnetic circular dichroism (MCD) spectrum showed a W-shaped feature in the Soret-band region.[9] These results imply the formation of a high-spin Fe^{3+} complex with the phenolate oxygen ligand of Y161, which is quite consistent with that found in the crystal structure.[3,4]

rHSA(B)−hemin did not exhibit the CT band because of the Y161L mutation and was easily reduced to the corresponding ferrous complex by adding a small molar excess amount of aqueous $Na_2S_2O_4$ under an Ar atmosphere. A single broad absorption band (λ_{max} = 559 nm) in the α,β region was very similar to that of deoxy Mb and indicated the formation of a five-N-coordinate Fe^{2+} complex (Figure 2).[10] The spectral pattern was unaltered in the temperature range of 0−25 °C. The shape of the asymmetric MCD spectrum also resembled that of deoxy Mb.[11] This suggests that the heme is accommodated into the tailor-made heme pocket with an axial coordination involving His-142.

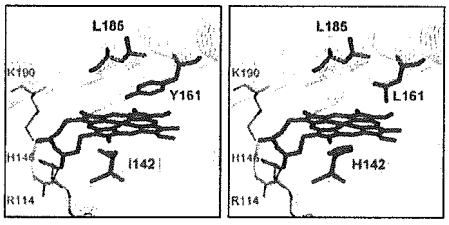

rHSA(wt) I142, Y161 rHSA(B) I142H/Y161L

Figure 1. Prosthetic heme group complexed within the heme pocket in subdomain IB of rHSA(wt) and rHSA(B) mutant produced on the basis of the crystal structure coordinate of the rHSA−hemin complex (ref 4).

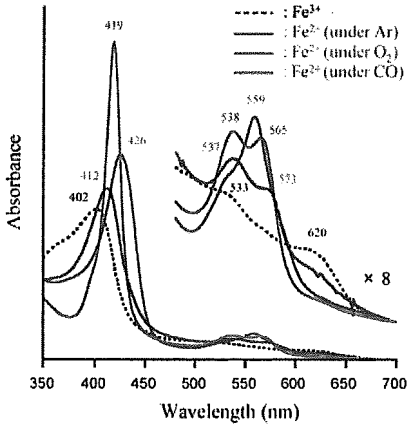

Figure 2. UV−vis absorption spectral changes of rHSA(B)−heme in phosphate buffered solution (pH 7.0, 50 mM) at 8 °C.

Upon exposure of the rHSA(B)−heme solution to O_2 gas, the UV−vis absorption changed to that of the dioxygenated complex (λ_{max} = 412, 537, 573 nm) at 0−25 °C[10] (lifetime of the O_2−adduct: ca. 10 min). After exposure to flowing CO, the heme produced a typical carbonyl complex (λ_{max} = 419, 538, 565 nm).

On the contrary, rHSA(A)−heme could not bind O_2 even at low temperature (~0 °C). It can be thought that the polar phenolate residue at the top of the porphyrin platform is likely to accelerate the proton-driven oxidation of the Fe^{2+} center. Replacing Y161 by

† Waseda University.
‡ Imperial College London.

10.1021/ja046022t CCC: $27.50